Editors' Suggestion

Cooper pairing of incoherent electrons: An electron-phonon version of the Sachdev-Ye-Kitaev model

Ilya Esterlis[1] and Jörg Schmalian[2,3]

[1]*Department of Physics, Stanford University, Stanford, California 94305, USA*

[2]*Institute for Theory of Condensed Matter, Karlsruhe Institute of Technology, Karlsruhe 76131, Germany*

[3]*Institute for Solid State Physics, Karlsruhe Institute of Technology, Karlsruhe 76021, Germany*

(Received 11 June 2019; revised manuscript received 14 August 2019; published 16 September 2019)

We introduce and solve a model of interacting electrons and phonons that is a natural generalization of the Sachdev-Ye-Kitaev model and that becomes superconducting at low temperatures. In the normal state, two non-Fermi-liquid fixed points with distinct universal exponents emerge. At weak coupling, superconductivity prevents the onset of low-temperature quantum criticality, reminiscent of the behavior in several heavy-electron and iron-based materials. At strong coupling, pairing of highly incoherent fermions sets in deep in the non-Fermi-liquid regime, a behavior qualitatively similar to that in underdoped cuprate superconductors. The pairing of incoherent time-reversal partners is protected by a mechanism similar to Anderson's theorem for disordered superconductors. The superconducting ground state is characterized by coherent quasiparticle excitations and higher-order bound states thereof, revealing that it is no longer an ideal gas of Cooper pairs, but a strongly coupled pair fluid. The normal-state incoherency primarily acts to suppress the weight of the superconducting coherence peak and reduce the condensation energy. Based on this, we expect strong superconducting fluctuations, in particular at strong coupling.

DOI: 10.1103/PhysRevB.100.115132

I. INTRODUCTION

Superconductivity is the ultimate fate of a Fermi liquid at low temperatures [1–4]. A key assumption that gives rise to this Cooper instability is that the excitations of a Fermi liquid are slowly decaying Landau quasiparticles with the same quantum numbers as free fermions. The resulting superconducting ground state can be understood as an ideal gas of Cooper pairs. Since superconductivity occurs in many systems where such sharp excitations are absent, the conditions for pairing of incoherent electrons is an important open problem. The emergence of a sharp superconducting coherence peak of small weight from a broad and structureless normal-state spectrum is in fact one of the hallmarks of the cuprate superconductors [5–9], where the weight of the coherence peak was shown to be strongly correlated with the superfluid stiffness and the condensation energy [9]. Key questions in this context are as follows: Can one form Cooper pairs from completely incoherent fermions? What is the role of quantum criticality for pairing? Are there sharp quasiparticles in such a superconductor? Is the Cooper pair fluid that emerges still an ideal gas of pairs?

To address these questions in a theoretically well-controlled way, it is highly desirable to identify a solvable model for nonquasiparticle superconductivity. A crucial issue is the proper interplay of non-Fermi-liquid excitations and the pairing interaction. For example, the spectral function of a Fermi liquid right at the Fermi surface,

$$A_{\mathrm{FL}}(\omega) = Z_{\mathrm{FL}}\delta(\omega), \tag{1}$$

is expected to transform for a quantum-critical system to the power-law form

$$A_{\mathrm{QC}}(\omega) = A_0|\omega|^{2\Delta-1} \tag{2}$$

with exponent Δ. For $\Delta > 0$ an evaluation of the pairing susceptibility with instantaneous pairing interaction yields no Cooper instability [10–12]. Superconductivity would then only occur if the pairing interactions exceeded a threshold value. Then, a superconducting ground state would be the exception rather than the rule. However, for a number of systems near a fermionic quantum-critical point, ranging from composite-fermion metals, high-density quark matter to metals with magnetic or nematic critical points, the self-consistently determined pairing interaction inherits a singular behavior

$$V_{\mathrm{pair}}(\omega) = V_0|\omega|^{1-4\Delta} \tag{3}$$

with the same exponent Δ [13–25]. The singular pairing interaction compensates for the weakened ability of non-Fermi-liquid (NFL) electrons to form Cooper pairs. One obtains a generalized Cooper instability and superconductivity for infinitesimal V_0. These considerations already demonstrate that there is a fundamental distinction between a pairing interaction that is unrelated to or directly linked to the cause of non-Fermi-liquid physics. A particularly dramatic phenomenon is the pairing of fully incoherent non-Fermi-liquid states, e.g., systems with a flat and structureless spectral function

$$A_{\mathrm{IC}}(\omega) = A_0 + \cdots. \tag{4}$$

The pairing of such fully incoherent fermions remains an open question. It corresponds to the extreme limit of $\Delta = \frac{1}{2}$ of the quantum-critical pairing problem.

Significant progress in our understanding of quantum-critical superconductivity was achieved because of advances to formulate models that allow for sign-problem free quantum Monte Carlo simulations [26–34]. The appeal of these

computational approaches is that they allow for a detailed analysis of the interplay between quantum criticality, pairing, and other competing states of matter. Advances have also been made in clearly specifying how one would sharply distinguish the pairing state of a non-Fermi liquid from the more conventional one. Cooper pairing of quantum-critical fermions and incoherent pairing should be discernible by analyzing the frequency and temperature dependence of the dynamical pair susceptibility [18,19,35], a quantity accessible through higher-order Josephson effects.

An interesting approach that yields non-Fermi-liquid behavior is provided by the Sachdev-Ye-Kitaev (SYK) model [36–40] and generalizations thereof [41–47]. The SYK model describes N fermions with a random, infinite-ranged interaction and gives rise to a critical phase where fermions have a vanishing quasiparticle weight at low energies and temperatures. The model is exactly solvable in the limit of infinitely many fermions, $N \to \infty$, yielding a tractable example of strong-coupling, non-Fermi-liquid behavior. The SYK model is appropriate for situations where interactions dominate over the kinetic energy. Thus, it could serve as a toy model for systems that are characterized by flat bands, such as cuprate superconductors for momenta near the antinodal points or possibly twisted bilayer graphene near the magic angle [48]. Formulated as a model with infinite-range interactions it can alternatively be understood either as a mean-field approach that ignores strong spatial fluctuations, akin to the dynamical mean-field theory of correlated electron systems [49,50], or as a local quantum dot system with an abundance of internal degrees of freedom and weak interdot coupling [46,47]. Either point of view implies that results obtained within the SYK approach are likely to capture important aspects of strong correlations in finite-dimensional systems at intermediate energies. The randomness of the model, that is crucial for the formal development of the theory, may be understood as simulating real disorder or rather be an effective description of a clean system with a rich spectrum of low-energy excitations. Such self-generated randomness is a phenomenon known to emerge in strongly frustrated classical and quantum systems [51,52]. Another appeal of this model is that its gravity dual is an asymptotic anti–de Sitter space AdS_2 that can be explicitly constructed [40,42], an approach that is particularly promising if one wants to include fluctuations that go beyond the leading large-N limit [53,54].

An exciting question is whether one can construct superconducting versions of the SYK model and address the question of how pairing occurs in such a non-Fermi-liquid state of matter. Indeed, in Ref. [55] Patel *et al.* added an additional pairing interaction to the model and demonstrated that an instantaneous attractive coupling induces a large superconducting gap in the spectrum. This describes the behavior of a non-Fermi liquid toward Cooper pairing due to an interaction that is unrelated to the initial cause of non-Fermi-liquid behavior. In another setting, of neutral fermions coupled to a single site of an "ordinary" complex spinless fermion, odd-frequency superconductivity was recently discussed in Ref. [56]. It was also shown recently by Wang in Ref. [95] that superconductivity can emerge at $O(1/N)$ in a model similar to that discussed here (but in which superconductivity is absent in the large-N limit).

A fundamental question is to understand systems where the interaction that causes the breakdown of the quasiparticle description is equally responsible for pairing. Such quantum-critical pairing is then directly linked to the non-Fermi-liquid state. As we will see, the SYK strategy allows to construct a solvable model of superconductivity near a quantum-critical point. It can directly address the issue of a generalized Cooper instability with enhanced pairing interaction balancing the weakened ability of non-Fermi-liquid states to form pairs; see Eq. (3). Such a model also has the potential to deepen our understanding of holographic superconductivity [57–59]. The SYK model offers an explicit gravity dual that will have to display an instability due to the onset of superconductivity.

In this paper we present a model of electrons interacting with phonons via a random, infinite-range coupling. It is well established that singlet superconductivity can easily be destroyed if one breaks time-reversal symmetry. Thus, we consider a distribution function of real-valued electron-phonon coupling constants. This will indeed give rise to superconductivity in the SYK model at leading order in an expansion for large number of fermions and bosons. The well-known Eliashberg equations of superconductivity [60–62], yet with self-consistently determined electron and phonon propagator, turn out to be exact.

We find a superconducting ground state for all values of the coupling constant. Our calculation reveals that superconductivity emerges very differently in the weak- and strong-coupling regimes of the model. At weak coupling T_c coincides, up to numerical prefactors, with the crossover from Fermi-liquid to non-Fermi-liquid behavior. Such behavior, where superconductivity preempts the ultimate quantum-critical state, is reminiscent of that observed in heavy-electron [63–66] and iron-based [67–70] superconductors. Thus, the superconducting state masks large parts of the non-Fermi-liquid regime. Similar behavior was recently seen in quantum Monte Carlo simulations of spin-fluctuation-induced superconductivity [34]. At weak coupling we also reproduce a generalized Cooper instability of the type discussed in Eq. (3). The nature of the superconductivity changes in the strong-coupling regime, where pairing occurs deep in the non-Fermi-liquid state and T_c approaches a universal value times the bare phonon frequency. Pairing at strong coupling is a genuine example of Cooper pairs made up of completely ill-defined individual electrons, a phenomenon that is relevant for the underdoped cuprate superconductors. A model for incoherent fermions in the cuprates due to similarly soft bosons, that also gives rise to magnetic precursors, was discussed in Refs. [71,72] and is similar in spirit to the behavior found here in the strong-coupling regime. The resulting phase diagram that follows from our analysis is given in Fig. 1.

The results of this paper are determined from a model of electrons that interact strongly with soft lattice vibrations. In several instances we compare the qualitative features of our results with observations made in strongly correlated superconductors such as members of the heavy-fermion, iron-based, or cuprate family. Strong evidence exists that the pairing mechanism in these systems is predominantly of electronic origin. The findings of our analysis can, however, be rather straightforwardly extended to models of electrons that interact with collective electronic excitations, such as nematic

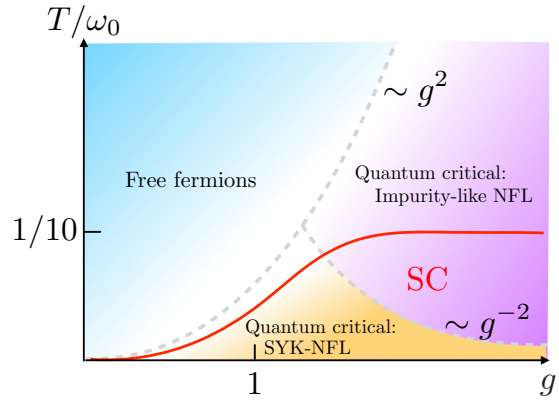

FIG. 1. Schematic phase diagram of the SYK model for electron-boson coupling as function of the dimensionless coupling constant $g = \bar{g}/\omega_0^{3/2}$, where ω_0 is the bare phonon frequency. At lowest T the normal state would be a non-Fermi-liquid state with anomalous exponents, similar to other SYK models. For $g < 1$ superconductivity sets in at $T_c/\omega_0 \propto g^2$, comparable to the temperature where quantum-critical SYK-NFL sets in. Thus, pairing occurs instead of the low-T quantum critical state. At strong coupling a new intermediate-temperature regime opens up that is characterized by fully incoherent fermions. Coherent pairing of such incoherent fermions is still possible with finite transition temperature $T_c \to 0.112\omega_0$.

or magnetic fluctuations; see also the summary section of this paper. In this more general reasoning we see the justification of our statements as they pertain to the aforementioned materials.

II. MODEL

We start from the following Hamiltonian:

$$H = -\sum_{i=1}^{N}\sum_{\sigma=\pm}\mu c_{i\sigma}^{\dagger}c_{i\sigma} + \frac{1}{2}\sum_{k=1}^{M}\left(\pi_k^2+\omega_0^2\phi_k^2\right) + \frac{\sqrt{2}}{N}\sum_{ij,\sigma}^{N}\sum_{k}^{M} g_{ij,k}c_{i\sigma}^{\dagger}c_{j\sigma}\phi_k, \tag{5}$$

with fermionic operators $c_{i\sigma}$ and $c_{i\sigma}^{\dagger}$ that obey $[c_{i\sigma}, c_{j\sigma'}^{\dagger}]_+ = \delta_{ij}\delta_{\sigma\sigma'}$ and $[c_{i\sigma}, c_{j\sigma}]_+ = 0$ with spin $\sigma = \pm 1$. In addition, we have phonons, i.e., scalar bosonic degrees of freedom ϕ_k with canonical momentum π_k, such that $[\phi_k, \pi_{k'}]_- = i\delta_{kk'}$. Here, $i, j = 1 \ldots N$ refer to fermionic modes and $k = 1 \ldots M$ to the phonon field. Below we consider the limit $N = M \to \infty$. We briefly comment on the behavior for arbitrary M/N in Appendix C. For simplicity, we assume particle-hole symmetry which yields $\mu = 0$ for the chemical potential. Notice, the coupling to phonons usually shifts the particle-hole symmetric point to a nonzero value of μ. This is a consequence of the Hartree diagram. However, this contribution vanishes in the $N \to \infty$ limit.

The electron-phonon coupling constants $g_{ij,k}$ are real, Gaussian-distributed random variables that obey

$$g_{ij,k} = g_{ji,k}. \tag{6}$$

The distribution function has zero mean and a second moment $|g_{ij,k}|^2 = \bar{g}^2$. The unit of $\bar{g}$ is energy$^{3/2}$. Thus, even for $\mu = 0$, the model has two energy scales, the bare phonon frequency ω_0 and $\bar{g}^{2/3}$. For convenience we measure all energies and temperatures in units of ω_0 and use the dimensionless coupling constant $g^2 = \bar{g}^2/\omega_0^3$. Whenever it seems useful, we will reintroduce ω_0 in the final results.

We perform the disorder average using the replica trick [73]. Since $g_{ij,k}$ only occurs in the random part of the interaction we are interested in the following average:

$$\overline{e^{-S_{\rm rdm}}} = \overline{e^{-\sum_{ijk} g_{ijk}O_{ijk}}}, \tag{7}$$

where $O_{ijk} = \frac{\sqrt{2}}{N}\sum_{\sigma a}\int_0^\beta d\tau\, c_{i\sigma a}^{\dagger}(\tau)c_{j\sigma a}(\tau)\phi_{ka}(\tau)$. Here, $a = 1, \ldots, n$ stands for the replica index and the overbar denotes disorder averages, while τ stands for the imaginary time in the Matsubara formalism with $\beta = (k_B T)^{-1}$ the inverse temperature. The $g_{ij,k}$ are for given k chosen from the Gaussian orthogonal ensemble (GOE) of random matrices [74]. We obtain for the disorder average

$$\overline{e^{-\sum_{ijk} g_{ijk}O_{ijk}}}|_{\rm GOE} = e^{\bar{g}^2\sum_{ijk}(O_{ijk}^{\dagger}+O_{ijk})^2}. \tag{8}$$

There is an important distinction between the models with and without time-reversal symmetry for individual disorder configurations. If we allow for complex coupling constants with $g_{ij,k} = g_{ji,k}^*$, then, for given k, $g_{ij,k}$ would be chosen from the Gaussian unitary ensemble (GUE). Performing the disorder average for the case of the unitary ensemble yields

$$\overline{e^{-\sum_{ijk} g_{ijk}O_{ijk}}}|_{\rm GUE} = e^{2\bar{g}^2\sum_{ijk} O_{ijk}^{\dagger}O_{ijk}}. \tag{9}$$

As can be seen from the distinct behavior of the disorder averages in Eqs. (9) and (8), the orthogonal ensemble with time-reversal symmetry contains, in addition to terms like $O_{ijk}^{\dagger}O_{ijk}$, that also occur in the unitary ensemble, the anomalous terms $O_{ijk}^{\dagger}O_{ijk}^{\dagger}$ and $O_{ijk}O_{ijk}$. The anomalous terms can be analyzed at large N by introducing anomalous propagators and self-energies. These terms give rise to superconductivity (see Appendix A).

The subsequent derivation of the self-consistency equations of the model in the large-N limit proceeds along the lines of other SYK models [36,39–43,55,56]. Assuming replica diagonal solutions, we obtain a coupled set of equations for the fermionic and bosonic self-energies and Green's functions. This derivation is summarized in Appendix A. The most straightforward formulation can be performed using the Nambu spinors $c_i = (c_{i\uparrow}, c_{i\downarrow}^{\dagger})$ in the singlet channel. Then, we obtain the coupled set of equations for the self-energies:

$$\hat{\Sigma}(\tau) = \bar{g}^2\tau_3\hat{G}(\tau)\tau_3 D(\tau), \tag{10}$$

$$\Pi(\tau) = -\bar{g}^2{\rm tr}(\tau_3\hat{G}(\tau)\tau_3\hat{G}(\tau)), \tag{11}$$

with $D^{-1}(\nu_n) = \nu_n^2 + \omega_0^2 - \Pi(\nu_n)$ and the fermionic Dyson equation in Nambu space $\hat{G}(\epsilon_n)^{-1} = i\epsilon_n\tau_0 + \mu\tau_3 - \hat{\Sigma}(\epsilon_n)$, where τ_α are the 2×2 Pauli matrices in Nambu space. Here, $\epsilon_n = (2n+1)\pi T$ and $\nu_n = 2n\pi T$ are fermionic and bosonic Matsubara frequencies, respectively. These relations correspond to the Eliashberg equations of electron-phonon superconductivity, however, with the inclusion of the fully

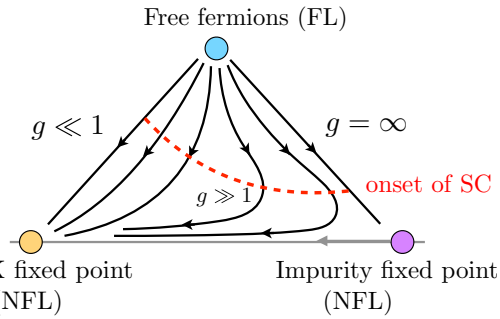

FIG. 2. Renormalization group flow that summarizes the physics of the phase diagram of Fig. 1. The free-fermion fixed point is always unstable and flows at low energies to the quantum-critical SYK fixed point. At strong coupling, the flow is influenced for a large energy window by a new strong-coupling fixed point of fully incoherent fermions. At $g = \infty$ this impuritylike fixed point is stable and governs the behavior at all scales. Superconductivity, marked by the red line, at strong coupling occurs in the vicinity of the impuritylike fixed point. At weak coupling it sets in at the crossover between the two fixed points.

renormalized boson self-energy. We use the standard parametrization for $\hat{\Sigma}$ in Nambu space [60–62]:

$$\hat{\Sigma}(\epsilon_n) = \Sigma(\epsilon_n)\tau_0 + \Phi(\epsilon_n)\tau_1, \tag{12}$$

where we dropped the terms proportional to τ_3 and τ_2 due to our assumption of particle-hole symmetry and by fixing the phase of the superconducting wave function, respectively. We will also frequently use the parametrization

$$\Sigma(\epsilon_n) = i\epsilon_n[1 - Z(\epsilon_n)], \tag{13}$$

where $Z(\epsilon_n)^{-1}$contains information about the quasiparticle weight.

III. NON-FERMI-LIQUID FIXED POINTS IN THE NORMAL STATE

We first solve the coupled equations in the normal state, i.e., assuming that the anomalous self-energy vanishes: $\Phi = 0$. As discussed above, this corresponds to the full solution of a model that breaks time-reversal symmetry for individual configurations of the $g_{ij,k}$, chosen from the unitary ensemble. We obtain the following coupled equations for the fermionic and bosonic self-energies:

$$\Sigma_\sigma(\tau) = \bar{g}^2 G_\sigma(\tau) D_0(\tau), \tag{14}$$

$$\Pi(\tau) = -\bar{g}^2 \sum_\sigma G_\sigma(\tau) G_\sigma(-\tau), \tag{15}$$

as well as the Dyson equations $G_\sigma^{-1}(\epsilon_n) = i\epsilon_n + \mu - \Sigma_\sigma(\epsilon_n)$ and $D^{-1}(\nu_n) = \nu_n^2 + \omega_0^2 - \Pi(\nu_n)$. As sketched in Fig. 2, these coupled equations give rise to two distinct non-Fermi-liquid fixed points that govern the low-temperature regime for all coupling constants and the intermediate temperature regime at strong coupling, respectively. In what follows we will summarize the key properties of these fixed points, while a detailed derivation of our results can be found in Appendix B.

A. Low-temperature behavior: Quantum-critical SYK fixed point

We first discuss the solution of this coupled set of equations at low temperatures. The key finding is the following form of the fermionic and bosonic propagators on the Matsubara axis:

$$G(\epsilon_n) = \frac{1}{i\epsilon_n\left(1 + c_1\left|\frac{g^2}{\epsilon_n}\right|^{2\Delta}\right)}, \tag{16}$$

$$D(\nu_n) = \frac{1}{\nu_n^2 + \omega_r^2 + c_3\left|\frac{\nu_n}{g^2}\right|^{4\Delta-1}}. \tag{17}$$

Here,

$$\omega_r^2 = c_2(T/g^2)^{4\Delta-1} \tag{18}$$

is the renormalized phonon frequency. The c_i are numerical coefficients of order unity. The value of the exponent Δ is generally confined to the interval $\frac{1}{4} < \Delta < \frac{1}{2}$, and for our problem we find

$$\Delta \backsimeq 0.420374134464041. \tag{19}$$

In Appendix B we derive these results, demonstrate that they agree very well with our numerical solution of Eqs. (14) and (15), and give analytic and numeric expressions for the coefficients $c_i(\Delta)$. With Δ of Eq. (19) we find $c_1 \approx 1.154\,700$, $c_2 \approx 0.561\,228$, and $c_3 \approx 0.709\,618$.

The findings of Eqs. (16)–(18) are summarized in Fig. 3, where these equations have been analytically continued from the imaginary to the real frequency axis. Let us discuss the main implications of these findings. The fermionic propagator (16) is similar to solutions of other SYK models and at low energies is dominated by the self-energy

$$\Sigma(\epsilon_n) = -i\,\mathrm{sign}(\epsilon_n) c_1 g^{4\Delta} |\epsilon_n|^{1-2\Delta}, \tag{20}$$

with anomalous exponent Δ. Only the numerical value of Δ is different from what can be found in purely fermionic models. Notice, however, that we can vary Δ in the intervals $(\frac{1}{4}, \frac{1}{2})$ if we vary the ratio M/N of the number of bosonic and fermionic degrees of freedom (see Appendix C and Ref. [45]). The bosonic propagator (17) is, at low frequencies, dominated by an anomalous Landau damping term, caused by the coupling to fermions and hence determined by the same anomalous exponent Δ.

Notice that the system is critical for all values of ω_0 and g. This is a surprising result. The renormalized phonon frequency

$$\omega_r^2 = \omega_0^2 - \Pi(0) \tag{21}$$

in Eq. (18) always vanishes as $T \to 0$. One might have expected that $\Pi(0)$ compensates the bare mass only for one specific value of the coupling constant g, which would then determine a quantum-critical point. Instead, the system remains critical for all values of g, i.e., the fixed point described by Eqs. (16) and (17) is stable (see Fig. 2). This stability is a consequence of the diverging charge susceptibility of bare fermions with $G(i\epsilon_n)^{-1} \approx i\epsilon_n$. It is the non-Fermi-liquid state that lifts the degeneracy of the local Fermi liquid and protects the system against diverging charge fluctuations.

The scaling solution in Eqs. (16) and (17) is valid in a low-temperature regime $T \lesssim T^*$ where the self-energies

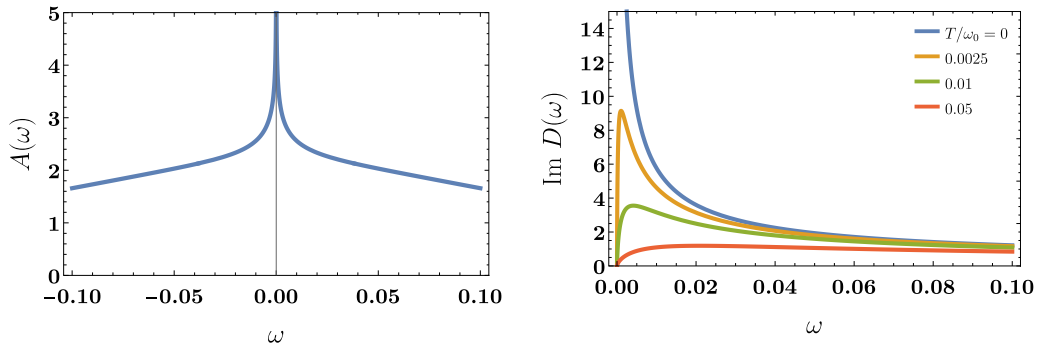

FIG. 3. Spectral function $A(\omega) = -\frac{1}{\pi}\mathrm{Im}G(\omega)$ and imaginary part of the bosonic propagator on the real frequency axis for dimensionless coupling constant $g = 0.5$. The phonon spectrum is shown for several temperatures, displaying the softening of the phonon mode ω_r.

dominate the bare fermion and boson Green's functions. We can estimate this crossover temperature as

$$T^* = \min(T_f, T_b), \tag{22}$$

where $T_f \sim g^2\omega_0$ and $T_b \sim g^{-\phi}\omega_0$, where $0 < \phi = \frac{8\Delta-2}{3-4\Delta} \leqslant 2$ for the allowed values $\frac{1}{4} < \Delta \leqslant \frac{1}{2}$. Below we will see that the relevant exponent at large g is $\Delta = \frac{1}{2}$, so that $\phi = 2$. Thus, the SYK-type quantum-critical regime is confined to temperatures $T \lesssim g^2\omega_0$ at small g and $T \lesssim g^{-2}\omega_0$ at large g (see Fig. 1).

B. Intermediate-temperature behavior: Impuritylike non-Fermi-liquid fixed point

The quantum-critical regime of Eqs. (16) and (17) is, however, not the only universal non-Fermi-liquid regime of this model. Once $g > 1$ an increasingly wide intermediate-temperature window $g^{-2} < T < g^2$ opens up. In this new temperature window we find for the electron and phonon propagators the solution

$$G(\epsilon_n) = \frac{-2i\,\mathrm{sign}(\epsilon_n)}{\sqrt{\epsilon_n^2 + \Omega_0^2} + |\epsilon_n|}, \tag{23}$$

$$D(\nu_n) = \frac{1}{\nu_n^2 + \omega_r^2}, \tag{24}$$

with a large fermionic energy scale $\Omega_0 = \frac{16}{3\pi}g^2$ and small phonon energy

$$\omega_r^2 = \left(\frac{3\pi}{8}\right)^2 T/g^2. \tag{25}$$

The findings of Eqs. (23)–(25) are summarized in Fig. 4. Since $T \ll \Omega_0$ fermions are "cold" and effectively behave as if they were quantum critical with exponent $\Delta = \frac{1}{2}$, i.e., with impuritylike self-energy

$$\Sigma(\epsilon_n) = -i\,\mathrm{sign}(\epsilon_n)\frac{8}{3\pi}g^2. \tag{26}$$

Noninteracting electrons with static impurities give rise to a similar self-energy and can, for a given disorder configuration, be considered a Fermi liquid, essentially by definition. In our case, the situation is different. We have to analyze multiple phonon configurations, even for a given disorder configuration of the g_{ijk}. The resulting state cannot be mapped onto a free-fermion problem. Hence, the term non-Fermi liquid. The spectral function $A(\omega)$ is semicircular with a width $2\Omega_0$. The low-frequency spectral function is therefore frequency independent

$$A(|\omega| \ll \Omega_0) = \frac{3}{8g^2}, \tag{27}$$

reflecting the incoherent nature of the fermion spectrum, as mentioned in Eq. (4) in the Introduction. On the other hand, phonons are undamped but "hot," i.e., thermally excited since $T \gg \omega_r$ once $T \gg g^{-2}$. Given the large fermionic energy scale Ω_0 we can neglect Landau damping terms that we find to be $\propto|\omega_n|/\Omega_0$ in the intermediate energy window. While the phonons are sharp excitations with a strongly renormalized, soft frequency, the fermions are highly incoherent. Similar behavior was discussed in the context of magnetic precursors in cuprates [71,72]. The impuritylike behavior for the fermionic self-energy is expected given the quasistatic nature

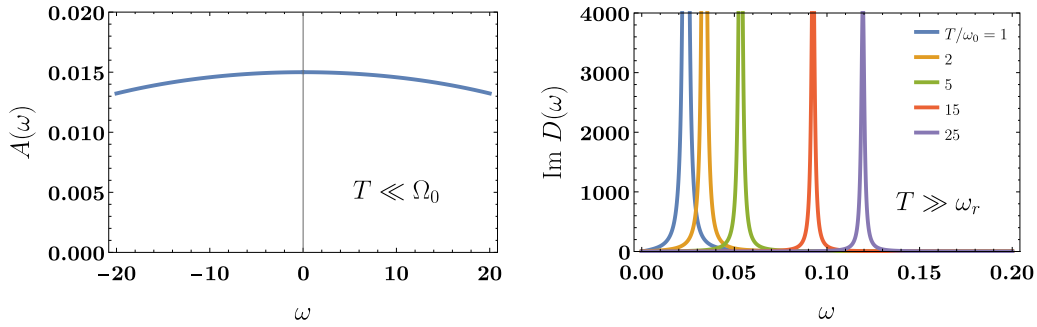

FIG. 4. Spectral function and imaginary part of the bosonic propagator on the real frequency axis and for dimensionless coupling constant $g = 5$. The phonon spectrum is shown for several temperatures, displaying the softening of the phonon mode ω_r.

of the phonons. Notice all these results correspond to an anomalous fermionic exponent $\Delta = \frac{1}{2}$. This strong-coupling fixed point is unstable and the system eventually crosses over to the low-temperature SYK fixed point. Only for $g = \infty$ does the impurity fixed point describe the ultimate low-T behavior (see Fig. 2). The analytic derivation of this strong-coupling criticality is summarized in Appendix B and compared with the full numerical solution of Eqs. (14) and (15).

IV. SUPERCONDUCTIVITY AND PAIRING OF NON-FERMI LIQUIDS

In the previous section we analyzed the behavior of the model (5) in the normal state. As indicated in Fig. 1 the normal state consists of three distinct regions that are separated by crossover lines. For $T > T_f \approx g^2\omega_0$ interaction effects are weak and we have essentially free electrons. For $T < T_f$ we have two distinct interacting regimes. At lowest temperatures with $T < T^* \sim \min(g^2\omega_0, g^{-2}\omega_0)$, quantum-critical behavior similar to that found in previous SYK-model calculations occurs, where phonons are characterized by anomalous Landau damping. For strong coupling, i.e., for $g > 1$, a new universal intermediate-temperature window $g^{-2} < T/\omega_0 < g^2$ opens up where strongly incoherent fermions interact with soft phonons.

Next, we allow for superconducting solutions and solve the coupled equations for the normal and anomalous self-energies. On the Matsubara axis, these coupled equations are

$$
\begin{aligned}
i\epsilon_n[1 - Z(\epsilon_n)] &= -\bar{g}^2 T \sum_{n'} \frac{D(\epsilon_n - \epsilon_{n'}) i\epsilon_{n'} Z(\epsilon_{n'})}{(\epsilon_{n'} Z(\epsilon_{n'}))^2 + \Phi(\epsilon_{n'})^2}, \\
\Phi(\epsilon_n) &= \bar{g}^2 T \sum_{n'} \frac{D(\epsilon_n - \epsilon_{n'}) \Phi(\epsilon_{n'})}{(\epsilon_{n'} Z(\epsilon_{n'}))^2 + \Phi(\epsilon_{n'})^2}, \\
\Pi(\nu_n) &= -2\bar{g}^2 T \sum_{n'} [G(\epsilon_{n'} + \nu_n) G(\epsilon_{n'}) \\
&\quad - F(\epsilon_{n'} + \nu_n) F(\epsilon_{n'})].
\end{aligned}
\tag{28}
$$

If we linearize the second equation with respect to the anomalous self-energy Φ and set $\Phi = 0$ in the first equation, we can determine the superconducting transition temperature. The result of this analysis is summarized in Fig. 5. First, our model does indeed give rise to a superconducting ground state for all values of the coupling constant $g > 0$. For small g the transition temperature behaves as

$$T_c(g \ll 1) \approx 0.16 g^2 \omega_0. \tag{29}$$

Thus, while T_c at weak coupling is numerically smaller than the crossover scale T^* to the quantum-critical regime, both temperature scales have the same parametric dependence. We will demonstrate in the next section that indeed superconductivity at $g < 1$ occurs near the onset of the low-T quantum-critical state. The behavior changes at strong coupling, where we find that

$$T_c(g \to \infty) \approx 0.11188 \omega_0 \tag{30}$$

approaches a finite value. In this case we form Cooper pairs deep in the non-Fermi-liquid state. We will analyze the behavior of this superconducting ground state and demonstrate

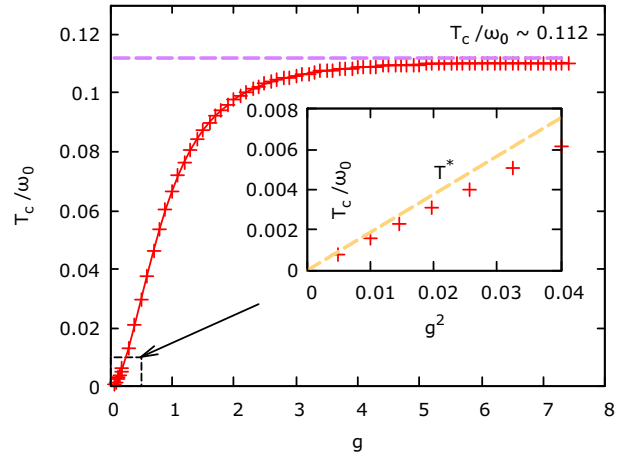

FIG. 5. Superconducting transition temperature as function of the coupling constant from the numerical solution of the coupled equations in the normal state and the analysis of the eigenvalue of the pairing vertex. At weak coupling we obtain $T_c \propto g^2\omega_0$, while the transition temperature saturates at strong coupling with $T_c(g \to \infty) \approx 0.112\omega_0$.

that it is characterized by a subtle formation of bound states of Cooper pairs with the dynamical pairing field.

In Eqs. (29) and (30) we give our results in terms of the bare phonon frequency ω_0 and the dimensionless coupling constant g. For any finite value of g the phonon frequency takes its bare value at sufficiently high temperature $T \sim g^2$. Thus, this frequency is in principle observable. However, in the large-g limit it is unclear whether this bare frequency can be recovered experimentally. The real observable is rather the renormalized frequency for temperatures of the order of T_c. Using our results for ω_r and the transition temperature, it follows $T_c/\omega_r \approx 0.284g$. In terms of the renormalized frequency, the transition temperature grows without bound [75].

For our subsequent discussion it is useful to express the pairing state in terms of the gap function

$$\Delta(\epsilon_n) = \Phi(\epsilon_n)/Z(\epsilon_n). \tag{31}$$

This yields the following coupled equations that are formally equivalent to Eq. (28):

$$
\begin{aligned}
Z(\epsilon_n) &= 1 + \bar{g}^2 T \sum_{n'} \frac{D(\epsilon_n - \epsilon_{n'})}{\sqrt{\epsilon_{n'}^2 + \Delta^2(\epsilon_{n'})}} \\
&\quad \times \left[\frac{1}{Z(\epsilon_{n'}) \sqrt{\epsilon_{n'}^2 + \Delta^2(\epsilon_{n'})}} \right] \frac{\epsilon_{n'}}{\epsilon_n}, \\
\Delta(\epsilon_n) &= \bar{g}^2 T \sum_{n'} \frac{D(\epsilon_n - \epsilon_{n'})}{\sqrt{\epsilon_{n'}^2 + \Delta^2(\epsilon_{n'})}} \left[\frac{1}{Z(\epsilon_{n'}) \sqrt{\epsilon_{n'}^2 + \Delta^2(\epsilon_{n'})}} \right] \\
&\quad \times \left(\Delta(\epsilon_{n'}) - \frac{\epsilon_{n'}}{\epsilon_n} \Delta(\epsilon_n) \right),
\end{aligned}
\tag{32}
$$

and the same equation for $\Pi(\nu_n)$. These equations are distinct from the usual Eliashberg theory where the momentum integration over states in a broad band replaces the terms in square brackets by $\pi\rho_0$, where ρ_0 is the density of states in the normal

state. In our problem we analyze systems with nondispersing bands, changing the character of the Eliashberg equations. We will see below that for very large g, where the interactions give rise to a significant broadening of the spectral function, we can replace the terms in square brackets by a spectral function $A(g\to\infty,\omega)=\frac{3}{8}g^{-2}$ times π. In this limit, some known results of the conventional Eliashberg theory [62,76–79] can be used to obtain a better understanding of the strong-coupling limit.

The appeal of the reformulation in terms of the gap function in Eq. (32) is that it clearly reveals the role of the zeroth bosonic Matsubara frequency for the gap equation. Suppose the bosonic propagator is dominated by the zeroth Matsubara frequency. This is the case at strong coupling where we obtained with Eqs. (24) and (25) that $D(\nu_m)$ is dominated by $\nu_m=0$, a result that led to the solutions of Eq. (23). From Eq. (32) it follows that there is no contribution to the pairing problem for $\epsilon_n=\epsilon_{n'}$. Thus, static phonons do not affect the onset of superconductivity. The same effect is also responsible for the Anderson theorem [80–85] where static nonmagnetic impurities will not affect the superconducting transition temperature. Soft phonons behave somewhat similar to nonmagnetic impurities [86,87]. Superconductivity is then only caused by the remaining quantum fluctuations of the phonons. How this happens and what the implications for the spectral properties of the superconducting state are will be discussed in the subsequent sections.

A. Superconductivity at weak coupling

We start our analysis of superconductivity in the weak-coupling regime $g<1$ and first estimate the superconducting transition temperature T_c from the linearized version of Eq. (28):

$$\Delta(\epsilon_n)=\bar{g}^2T_c\sum_{n'}\frac{D(\epsilon_n-\epsilon_{n'})}{Z(\epsilon_{n'})\epsilon_{n'}^2}\left(\Delta(\epsilon_{n'})-\frac{\epsilon_{n'}}{\epsilon_n}\Delta(\epsilon_n)\right), \tag{33}$$

where both $Z(\epsilon_n)$ and $D(\nu_n)$ are determined by our normal-state solutions (16) and (17). Here we use $\epsilon_nZ(\epsilon_n)=\epsilon_n+i\Sigma(\epsilon_n)$. For the phonon propagator of Eq. (17) we can safely neglect the ν_n^2 term in the denominator. When we explicitly write out the temperature dependence in the various terms we obtain the linearized gap equation

$$\Delta(\epsilon_n)=a_0\sum_{n'}\frac{\left(\frac{T_f}{T}\right)^{2\Delta}\mathrm{sign}(\epsilon_{n'})}{\left(\frac{T}{T_f}\right)^{2\Delta}\left|n'+\frac{1}{2}\right|+\left|n'+\frac{1}{2}\right|^{1-2\Delta}}\times\frac{\frac{\Delta(\epsilon_{n'})}{\epsilon_{n'}}-\frac{\Delta(\epsilon_n)}{\epsilon_n}}{m_0+|n-n'|^{4\Delta-1}},$$

with $m_0=\frac{c_2}{c_3(2\pi)^{4\Delta-1}}\approx 0.156\,558$, $a_0=\frac{1}{2\pi c_1^2c_2}\approx 0.212\,687$, and $T_f=\frac{1}{2\pi}c_1^{\frac{1}{2\Delta}}g^2\approx 0.1888g^2$. The temperature dependence of the gap equation only occurs in the combination T/T_f. Thus, the scale for the superconducting transition is set by T_f. However, this is precisely the temperature scale where the crossover between the univeral low-T non-Fermi-liquid fixed point and the high-temperature free-fermion behavior takes place. This is also the reason why we included the term $(\frac{T}{T_f})^{2\Delta}|n'+\frac{1}{2}|$ in the denominator, which corresponds to the bare fermionic propagator. Equally, the coefficient m_0 occurs as we have to include a finite phonon frequency at the transition temperature. If we keep all those terms, we obtain $T_c\approx 0.0821g^2$. Thus, we find that the transition temperature is about half of the crossover temperature T_f. The g^2 dependence agrees with our numerical finding shown in Fig. 5. Not surprisingly, the precise numerical coeffficient in T_c cannot be reliably determined as the transition temperature is right in the crossover regime between free-fermion and quantum-critical SYK behavior. The reason is that there appear to be corrections to the fermionic self-energy that are formally subleading at low frequencies, yet modify numerical coefficients. The correct behavior was obtained from the full numerical solution and yields Eq. (29); see also Fig. 5.

This analysis demonstrates that superconductivity in the weak-coupling regime occurs at the same temperature scale where quantum-critical non-Fermi-liquid behavior emerges. Thus, superconductivity occurs instead of the quantum-critical regime. While parametrically the same, the numerical coefficient of the transition temperature is somewhat smaller than the crossover scale T_f between the region of free-fermion and quantum-critical fermion behavior. Thus, in this regime it might be possible to observe quantum-critical scaling over a regime up to a decade in frequency or temperature. It should, however, not be possible to find several decades of universal scaling according to Eqs. (16) and (17). Superconductivity prevents such a wide quantum-critical regime.

Nevertheless, it is very instructive to compare our gap function with results from a previous analysis of the linearized gap equation in quantum-critical systems; see, in particular, Refs. [15,18,20–24]. If we formulate the linearized gap equation merely in terms of the universal contributions to the electron and phonon self-energies, we obtain

$$\Phi(\epsilon_n)=\frac{T_c}{c_1^2c_3}\sum_{n'}\frac{\Phi(\epsilon_{n'})}{|\epsilon_n-\epsilon_{n'}|^{4\Delta-1}|\epsilon_{n'}|^{2-4\Delta}}, \tag{34}$$

where $\epsilon_n=(2n+1)\pi T_c$. Here, we can see explicitly what was discussed in the Introduction, namely, that the singular pairing interaction $V_{\mathrm{pair}}(\nu_n)\propto D(\nu_n)\propto|\nu_n|^{1-4\Delta}$ compensates for the less singular fermionic propagator giving rise to a generalized Cooper instability. Self-consistency equations of this type have been discussed in the context of several scenarios for quantum-critical pairing in metallic systems [13–24]. In this equation, the entire T dependence disappears given that the two exponents in the denominator add up to unity. Thus, unless this equation is supplemented by appropriate boundary conditions, it is not possible to determine T_c (see Ref. [24]). This is achieved by our above solution of the gap equation for Δ_n. For a detailed discussion of the gap equation in the form (34), see Refs. [20–24].

In Fig. 6 we show the spectral function in the weak-coupling regime at low temperatures that was obtained from a numerical solution of the full coupled equations on the real frequency axis, following the approach of Refs. [88,89]. Our main observation is the emergence of a sharp excitation, and of several high-energy structures. We will discuss these high-energy shakeoff peaks in greater detail in the discussion of the strong-coupling limit. Finally, we observe that in this

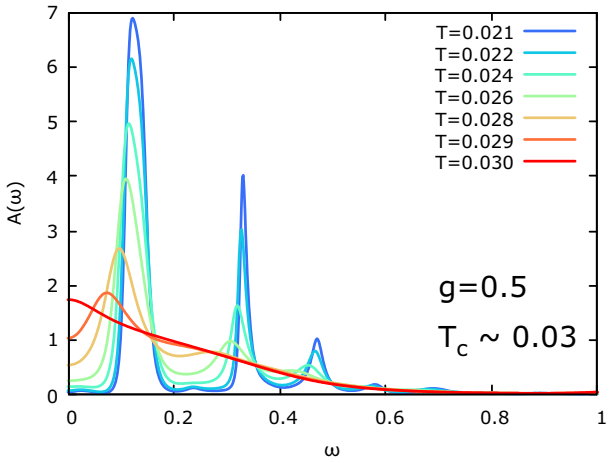

FIG. 6. Spectral function as function of temperature for $g = 0.5$. The superconducting transition temperature is $T_c = 0.03\omega_0$. We find higher-order bound states as well as a gap closing as function of temperature.

weak-coupling regime the superconducting gap closes as the temperature increases.

Overall, the analysis of the pairing problem in this weak-coupling regime closely resembles the behavior that was found in a number of metallic quantum-critical points [13–24]. The SYK model proposed here may serve as a starting point to go beyond the mean field limit and investigate the fluctuation corrections by following the advances in the $1/N$ corrections of SYK-type models [53,54].

B. Superconductivity at strong coupling

The investigation of superconductivity at strong coupling is of particular interest, as it reveals why fully incoherent fermions are able to nevertheless form a coherent superconducting state. We begin again with a determination of the superconducting transition temperature from the linearized gap equation. To this end, we start from Eq. (32) to obtain

$$\Delta(\epsilon_n) = \frac{3\pi}{8} T_c \sum_{n'} \frac{1}{(\epsilon_n - \epsilon_{n'})^2 + \omega_r^2} \times \left(\frac{\Delta(\epsilon_{n'})}{\epsilon_{n'}} - \frac{\Delta(\epsilon_n)}{\epsilon_n} \right) \mathrm{sign}(\epsilon_{n'}). \tag{35}$$

Here, we used the normal-state result (23) that has the low-frequency behavior

$$|\epsilon_n| Z(\epsilon_n) \approx \frac{8}{3\pi} g^2. \tag{36}$$

The large normal-state fermionic self-energy is responsible for the fact that the coupling constant g gets canceled in the prefactor of Eq. (35). The only dependence on the coupling constant in this equation is in the renormalized phonon frequency ω_r. At T_c, ω_r is determined by the normal-state solution of Eq. (25). However, since $T \gg \omega_r$ in the strong-coupling regime and since the zeroth Matsubara frequency does not contribute to superconductivity, we can simply set ω_r to zero in Eq. (35). The linearized gap equation becomes

$$\Delta_n = \alpha \sum_{n' \neq n} \frac{\frac{\Delta_{n'}}{2n'+1} - \frac{\Delta_n}{2n+1}}{(2n - 2n')^2} \mathrm{sign}\left(n' + \frac{1}{2} \right) \tag{37}$$

with $\alpha = \frac{3\omega_0^2}{8\pi^2 T_c^2}$. One easily finds that this equation has a solution for $\alpha_c \approx 3.034\,58$, which yields for the transition temperature $T_c = \sqrt{\frac{3\omega_0^2}{8\pi^2 \alpha_c}}$. Inserting the numerical coefficients yields Eq. (30). The transition temperature saturates as $g \to \infty$, in quantitative agreement with the numerical results shown in Fig. 5. This analysis also reveals the reason why pairing of fully incoherent fermions is possible. The lack of fermionic coherence, with large imaginary part of the electronic self-energy, is caused by the coupling to almost static bosonic modes. However, by arguments that in the context of disordered superconductors give rise to the Anderson theorem, such static bosons affect the normal and anomalous self-energies Σ and Φ, yet they cancel for the actual pairing gap $\Delta = \Phi/Z$ which is solely affected by the much weaker quantum fluctuations of the bosonic spectrum. Thus, pairing of time-reversal partners occurs even for incoherent fermions, a state that is protected by the same mechanism that makes the superconducting transition temperature robust against nonmagnetic impurities [80–87].

Now that we established that superconductivity sets in at a temperature that is deep in the incoherent strong-coupling regime, we discuss the properties of this superconducting state. We start with our numerical results for the spectral function and the anomalous Green's function. In Fig. 7 we show the fermionic spectral function in the superconducting state. In contrast to the gap-closing behavior that occurs at weak coupling, we find a filling of the gap, where the position of the maximum is essentially unchanged with temperature. In addition, higher-order shakeoff peaks occur that become most evident in the strong-coupling limit. The value of the superconducting gap is, just like the transition temperature, independent of coupling constant and of order of the bare phonon frequency ω_0. The lowest excitation of the fermions is $\Delta_0 \approx 0.640\,869\,140\,625\omega_0$. This yields

$$2\Delta_0/T_c \approx 11.456\,366, \tag{38}$$

which is more than three times the BCS value $2\pi e^{-\gamma_E} \approx 3.527\,754$. Such large values of $2\Delta_0/T_c$ have been obtained in the Eliashberg theory at strong coupling and for small phonon frequencies [61,62]; for a recent discussion, see [90]. Since the spectral weight of the excited state is transferred from energies below the gap, we can estimate the weight of the peak as $Z_{\mathrm{coh}} \approx \int_0^{\Delta \approx \omega_0} A_{\mathrm{ns}}(\omega) d\omega \propto g^{-2}$, where we used the normal-state spectral function of Eq. (27). We will see below that this result can be obtained rigorously at large g.

A very intriguing feature of the low-T spectral function is the occurrence of a large number of shakeoff peaks at discrete energies Ω_l that are reminiscent of the satellites that emerge as one forms polaronic states due to strong electron-phonon coupling. However, in the conventional polaronic theory these shakeoff structures exist at energies $\epsilon_0 + l\omega_r$ where ϵ_0 is the bare fermion energy, ω_r the phonon frequency [91], and l an

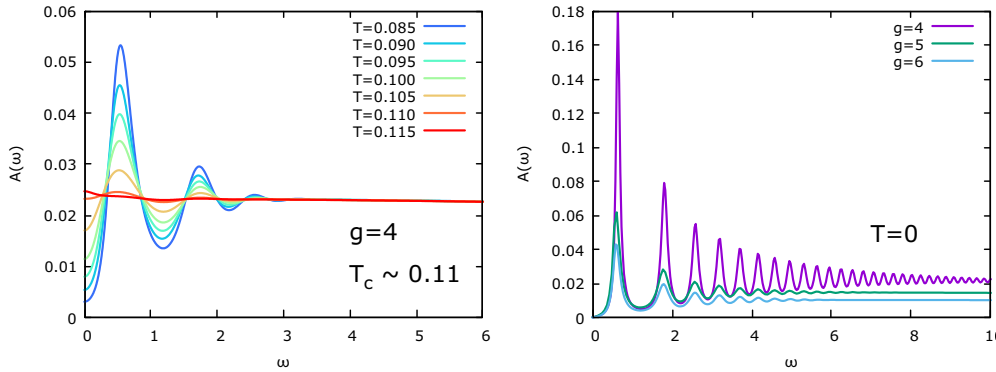

FIG. 7. Left panel: spectral function at strong coupling ($g = 4$ with $T_c \approx 0.11\omega_0$) for different temperatures. In distinction to the weak-coupling case we find gap filling, rather than gap closing, and a pronounced peak-dip-peak structure. The latter is not due to the coupling to the phonon mode, which has much smaller energy. Right panel: spectral function at $T = 0$ for different coupling constants revealing a large number of shakeoff peaks that reflect the bound-state formation in this limit of strongly coupled Cooper pairs. Also, the total weight of the leading coherence peak decreases with increasing coupling strength.

integer. In our case, ω_r is much smaller than the separation of the peaks in the spectral function. In fact, such structures in the normal and anomalous Green's function (see Fig. 8) have already been discussed in the context of strong-coupling solutions of the Eliashberg theory [77–79] and can be considered as self-trapping states of excited quasiparticles in the pairing potential of the other electrons [79]. The excited quasiparticle polarizes the pairing field, that deforms and traps it. The positions of the peaks are not equidistant. Following Ref. [79] we find at large l that the energies grow as $\Omega_l \approx \frac{\sqrt{3}\pi}{4}\sqrt{2l-1}\omega_0$. The first 10 peaks are located at $\Omega_l = p_l\Delta_0$ with $p_l \approx (1., 2.81, 4.05, 5.00, 5.76, 6.47, 7.14, 7.71, 8.29, 8.81)$. The first peak corresponds of course to the gap $\Omega_1 = \Delta_0$. These features are a clear sign of the fact that we have strongly interacting Cooper pairs, instead of an ideal gas of such pairs. While most of these shakeoff peaks smear out as the temperature increases (see left panel of Fig. 7) the first one or two peaks should be visible and serve as potential explanation for the observed peak-dip-hump structures seen in photoemission spectroscopy measurements of cuprate superconductors near the antinodal momentum [5–9].

One way to verify the emergence of these shakeoff peaks due to self-trapping in the pairing field is via the AC Josephson effect with current

$$I_J(t) = 2et_0^2[\mathrm{Re}\Pi_F(eV)\sin(2eVt) + \mathrm{Im}\Pi_F(eV)\cos(2eVt)], \tag{39}$$

where $\Pi_F(\omega)$ is the retarded version of the Matsubara function $\Pi_F(\nu_n) = T\sum_m F^\dagger(\epsilon_m)F(\epsilon_m - \nu_n)$. At low applied voltage $|eV| < 2\Delta_0$ the imaginary part of Π_F vanishes and the Josephson current is proportional to the sinus of the phase difference [92]. As the magnitude of the voltage exceeds $2\Delta_0$, an additional, phase-shifted AC Josepshon current that is proportional to $\cos(2eVt)$ sets in [93]. The coefficient is proportional to $\mathrm{Im}\Pi_F(eV)$ that we show in Fig. 9. Clearly, the sequence of bound states of the spectral function can be identified in the cosine AC Josephson response. Most interestingly, the sign change of two consecutive bound states, visible in the anomalous propagator in Fig. 8, directly leads to an alternating sign of the phase-shifted Josephson signal. This offers a way to identify the nature of higher-energy structures in the spectral function of superconductors, such as the bound states discussed here. For example, peaks in the spectral function due to multiple gaps on different Fermi surface sheets would not display such a sign-changing AC Josephson signal.

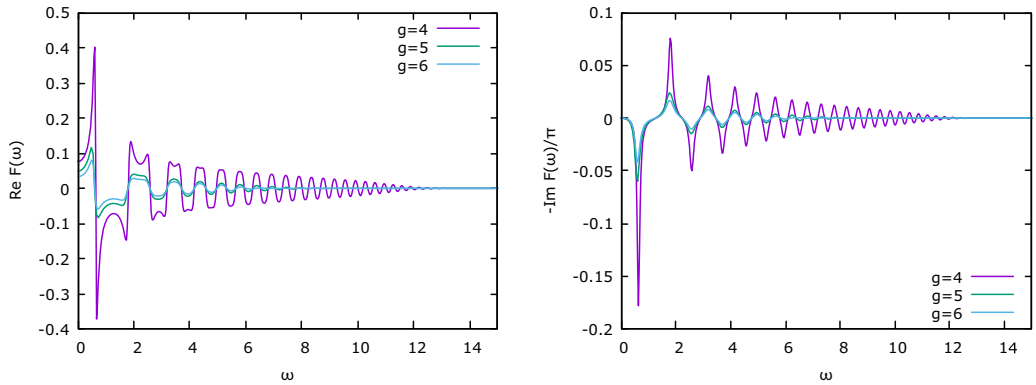

FIG. 8. Real part (left panel) and imaginary part (right panel) of the anomalous propagator $F(\omega)$ at $T = 0$ and for different coupling strengths. Notice the alternating sign of the peaks in the imaginary part.

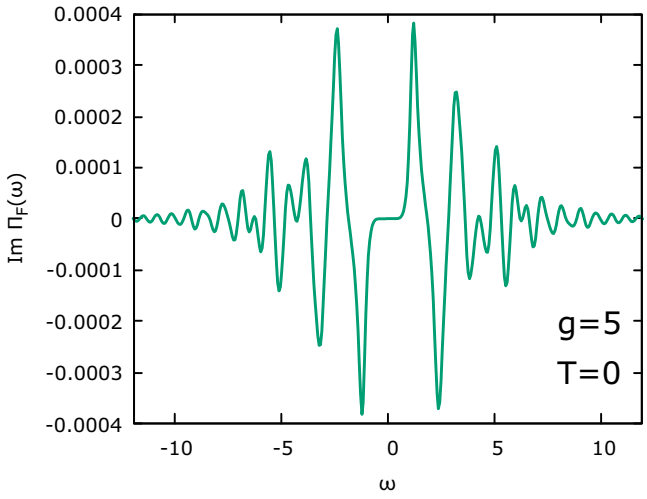

FIG. 9. Imaginary part of $\Pi_F(\omega)$ (defined in the text) for $g = 5$ at $T = 0$. $\mathrm{Im}\Pi_F(\omega)$ determines the amplitude of the phase-shifted AC Josephson current at higher voltage. The alternating sign of the peaks shown here is a direct consequence of the sign changes of consecutive peaks in the anomalous propagator, shown in Fig. 8. Thus, the AC Josephson response might serve as a tool to identify the internal structure of the Cooper pair states of a strongly coupled superconductor.

Finally, in Fig. 10 we show our results for the softening of the phonon frequency in the superconducting state. In the normal state the phonon mode is expected to soften, first according to Eq. (25) and below $T \sim \omega_0 g^{-2}$ according to Eq. (18). In the normal state, ω_r always vanishes for $T \to 0$. With the onset of superconductivity, the phonon frequency still decreases with decreasing T, however, it reaches a finite value ω_r^{sc} at $T = 0$. If we simply determine the phonon renormalization from the high-energy behavior of the spectral

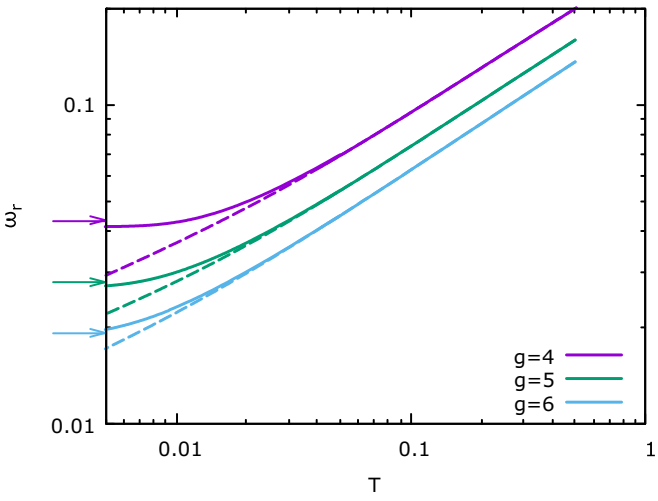

FIG. 10. Softening of the phonon frequency in the superconducting state at strong coupling. The dashed line is the normal-state result, continued below T_c. While in the normal state the phonon frequency vanishes as $T \to 0$, it approaches the finite $T = 0$ value $\omega_r^{sc} = \frac{\omega_0}{2}(\frac{3\pi}{8})^2 g^{-2}$, indicated by the arrows. Thus, both the electrons and the bosons are gapped in the superconducting state.

function in the superconducting state, we find $\omega_r^{sc} = \frac{\omega_0}{2}(\frac{3\pi}{8})^2 g^{-2}$ which agrees well with our numerical finding. As expected, the superconducting ground state has gapped fermion and phonon excitations which explains its coherent nature.

In the strong-coupling limit one can make contact with results that were obtained in the context of the usual Eliashberg theory, where conduction electrons with a large bandwidth require momentum averaging [60–62]. This additional momentum integration is not present in the SYK model, where one is interested in the behavior of strongly interacting narrow bands. From a purely technical point of view, the effect of the momentum integration in the usual Eliashberg formalism is to replace the term

$$\mathcal{A}(\epsilon_n) = \frac{1}{\pi}\frac{1}{Z(\epsilon_n)\sqrt{\epsilon_n^2 + \Delta^2(\epsilon_n)}}, \tag{40}$$

that occurs in square brackets in Eq. (32), by the normal-state density of states of the system. We will now show that at strong coupling the interaction-induced broadening plays a role similar to the momentum integration and we can replace $\mathcal{A}(\epsilon_n)$ by the broad spectral function of Eq. (27), i.e., $\mathcal{A}(\epsilon_n) \approx \frac{3}{8}g^{-2}$. To demonstrate this we take the $T = 0$ limit for $Z(\epsilon)$ in Eq. (32):

$$Z(\epsilon) = 1 + \bar{g}^2 \int \frac{d\epsilon'}{2\pi} \frac{1}{(\epsilon - \epsilon')^2 + \left(\omega_r^{sc}\right)^2} \times \frac{1}{Z(\epsilon')[\epsilon'^2 + \Delta^2(\epsilon')]} \frac{\epsilon'}{\epsilon}. \tag{41}$$

At large g the $T = 0$ phonon frequency is small and the sharp Lorentzian behaves as a δ function. Using our above result for ω_r^{sc} it follows that

$$Z(\epsilon) = 1 + \left(\frac{8g^2}{3\pi}\right)^2 \frac{1}{Z(\epsilon)[\epsilon^2 + \Delta^2(\epsilon)]}, \tag{42}$$

which yields at large g the solution

$$Z(\epsilon) = \frac{8g^2}{3\pi}\frac{1}{\sqrt{\epsilon^2 + \Delta^2(\epsilon)}}. \tag{43}$$

Thus, while $Z(\epsilon)$ and $\Delta(\epsilon)$ depend strongly on frequency in the superconducting state, the combination that enters $\mathcal{A}(\epsilon)$ is a constant. We have verified that this result for $Z(\epsilon)$ agrees very well with the full numerical solution for $g \gtrsim 4$. Using Eq. (43), the equation for the gap function is given as

$$\Delta(\epsilon_n) = \frac{3\pi}{8} T \sum_{n'} \frac{D(\epsilon_n - \epsilon_{n'})}{\sqrt{\epsilon_{n'}^2 + \Delta^2(\epsilon_{n'})}} \left(\Delta(\epsilon_{n'}) - \frac{\epsilon_{n'}}{\epsilon_n}\Delta(\epsilon_n)\right). \tag{44}$$

While the physics we are describing is rather different, formally this equation is identical to the usual Eliashberg theory, yet with a dimensionless coupling constant $\lambda = \frac{3}{8}$ and a very soft phonon frequency. If we set this phonon frequency to zero, the solution for $\Delta(\epsilon_n)$ is fully universal and independent of the coupling constant. Comparing with the numerical solution, we find that for $g \gtrsim 4$ this is indeed the case with high accuracy. Our result (30) can also be obtained from the well-known strong-coupling solution $T_c \approx 0.1827\sqrt{\lambda}\omega_0$ by Allen

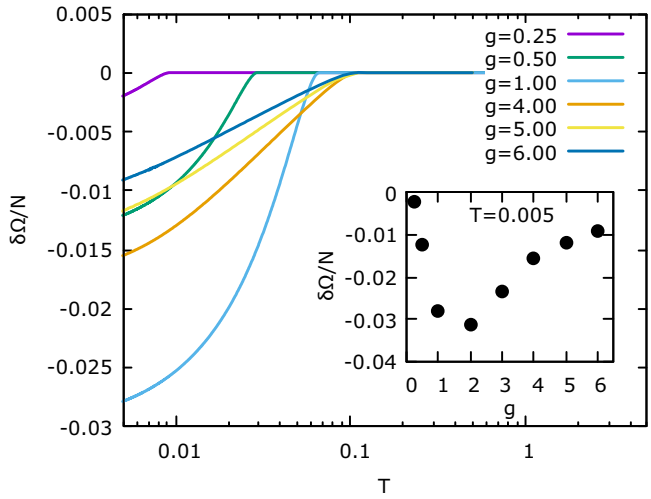

FIG. 11. Condensation energy $\delta\Omega/N$ as a function of temperature T for several values of g. The inset shows $\delta\Omega/N$ as a function of g at $T = 0.005\omega_0$.

and Dynes [76] if one inserts $\frac{3}{8}$ for the coupling constant. This is curious as one is very far from the applicability of this strong-coupling Allen-Dynes result for $\lambda = 0.375$. The reason we can apply this formula is because of the extreme softening of the phonons in our critical system. In the usual Eliashberg formalism, the frequency that enters the phonon propagator $D(\nu_n)$ is the bare, unrenormalized phonon frequency ω_0. Then, the Allen-Dynes limit of T_c only becomes relevant for extremely large values of the coupling constant.

Using Eq. (43) we can also find a very efficient way to relate the function $\Delta(\omega)$ on the real frequency axis and the spectral function

$$A(\omega) = \frac{3}{8g^2}\mathrm{Re}\left(\frac{\omega}{\sqrt{\omega^2 - \Delta(\omega)^2}}\right). \tag{45}$$

Since at large g the solution for the gap function is independent of the coupling constant, we immediately see that the weight of the superconducting coherence peak must scale as g^{-2}, a behavior that we estimated earlier based on the conservation of spectral weight. Thus, the key effect of the incoherent nature of the normal state is the reduced weight of the coherence peak, not its lifetime.

We finish this discussion with an analysis of the condensation energy as function of temperature and coupling strength. We determine the condensation energy $\delta\Omega$ from the difference of

$$\begin{aligned}\Omega/N = &-T\sum_n \mathrm{tr}\,\log\left(\hat{1} - \hat{G}_0(\nu_n)\hat{\Sigma}(\nu_n)\right)\\ &+\frac{T}{2}\sum_m \log[1 - D_0(\epsilon_m)\Pi(\epsilon_m)]\\ &-T\sum_n \mathrm{tr}(\hat{G}(\nu_n)\hat{\Sigma}(\nu_n))\end{aligned} \tag{46}$$

in the normal and superconducting state. Here, the trace is performed with respect to the degrees of freedom in Nambu space. As shown in Fig. 11, the temperature dependence of the condensation energy is very different in the weak- and strong-coupling regimes with an almost linear behavior down to very low T for large g. In this regime we also find a close relation between the condensation energy and the quasiparticle weight. At weak coupling $g < 1$ the magnitude of the condensation energy rises precipitously with increasing g. On the other hand, for $g \gtrsim 2$ the magnitude of the condensation energy drops slowly, consistent with the power-law dropoff of the quasiparticle weight. Such a correlation between coherent weight in the superconducting state and condensation energy has indeed been observed in the cuprate superconductors [9].

V. SUMMARY

In summary, we introduced and solved a model of interacting electrons and phonons with random, infinite-ranged couplings that is in the class of Sachdev-Ye-Kitaev models and allows for an exact solution in the limit of a large number of fermion and boson flavors. The normal-state phase diagram is summarized in Fig. 1 and contains adjacent to a high-energy regime of almost free fermions two distinct non-Fermi-liquid regimes. While the model starts out with a finite bare boson mass, soft, critical bosons are generated at low temperatures without fine tuning of the coupling strength. In addition to the usual SYK fixed point, characterized by power-law correlated bosons and fermions, we find an infinite-coupling fixed point that has no analog in the usual SYK formalism. It describes fully incoherent fermions and extremely soft yet sharp bosons. If the random electron-phonon interaction respects time-reversal symmetry not just on the average, but for each disorder configuration, the system becomes superconducting for all values of the coupling constant. Superconductivity not only emerges instead of non-Fermi-liquid behavior, an observation made in previous studies of two-dimensional systems [13–24] and reproduced in our weak-coupling regime, but also deep in the strong-coupling non-Fermi-liquid phase. The pairing state that we find is not an ideal gas of Cooper pairs like in the BCS theory or in the theory of preformed pairs undergoing Bose-Einstein condensation. Bound states of pairs explain the peak-dip-hump feature observed in the cuprates. Despite the incoherent nature of normal-state excitations, sharp, coherent excitations, including higher-order shakeoff peaks, emerge below T_c. The broader the fermionic states above T_c, the smaller the weight of the coherence peak below T_c. We established a direct quantitative connection between the degree of incoherency in the normal state and the reduced weight of a coherent Bogoliubov quasiparticle in the superconducting state, a correlation seen in experiments on the cuprates about two decades ago [9]. The superconducting transition temperature grows monotonically with coupling strength and levels off at a finite value that is determined by the bare phonon frequency. We remark that a general upper bound on T_c in conventional superconductors was recently proposed in Ref. [94], with the numerical value $T_c \lesssim \bar{\omega}/10$ comparable to the maximal T_c found here. The quantity $\bar{\omega}$ is an appropriately defined maximal renormalized phonon frequency. Given that for large g the bare and renormalized phonon frequencies at T_c are dramatically different, the comparison between these two bounds is at best possible for intermediate values of the coupling constant. In addition, the bound obtained in Ref. [94]

is ultimately due to polaron physics at strong coupling, which is absent in the $N \to \infty$ limit of the model considered here. In contrast to T_c, which grows with the coupling constant, we find the condensation energy is nonmonotonic and largest for intermediate-coupling strength $g \approx 1$. Thus, we expect strong fluctuations for large g if one goes beyond the leading large-N limit. Indeed, the appeal of the SYK formalism is that it offers a well-defined avenue to systematically improve the results (see, e.g., Refs. [53,54]).

The fact that we find superconductivity due to the same interactions that cause non-Fermi-liquid behavior leads to a puzzle in the holographic description of SYK. It implies that there must be unstable versions of nearly AdS_2 theories that yield superconductivity. Such instabilities are usually identified through the emergence of complex-valued scaling exponents [57–59]. Our results suggest to analyze whether such instabilities can be related to holographic superconductivity.

Our analysis can also be used as a starting point for lattice models of coupled strongly interacting superconductors and may be relevant in the theory of Josephson-junction arrays that are made up of unconventional superconductors. Finally, our analysis was performed for fermions that interact with a phonon mode, i.e., a scalar boson that couples to the fermion operator $c^\dagger_{i\sigma} c_{j\sigma}$ in the charge channel. It is straightforward to generalize the model and include a spin-1 boson $\boldsymbol{\phi}_k$ that couples to electrons via $g_{ij,k}\boldsymbol{\phi}_k \cdot \sum_{\sigma\sigma'} c^\dagger_{i\sigma}\boldsymbol{\sigma}_{\sigma\sigma'} d_{j\sigma'}$ with $\boldsymbol{\sigma}$ the vector of Pauli matrices in spin space and with two fermion species $c_{i\sigma}$ and $d_{j\sigma}$. These two fermion species correspond to different bands or different antinodal regions on the same band, depending on the problem under consideration. The large-N equations of this model are very similar to Eqs. (10) and (11), with $\tau_3 \to \tau_0$. The superconducting gap function of the two fermion species then has a relative minus sign, just like the gap function at the two antinodal points of a d-wave superconductor. The formal expression for the gap function turns out to be the same as the one discussed in this paper. Overall, the approach presented here is a promising starting point to understand superconductivity in strongly coupled, incoherent materials. It justifies some of the known results of the Eliashberg formalism, in particular, in the strong-coupling limit, and serves as a starting point to include fluctuations that go beyond the Eliashberg theory.

Note added. Recently, we learned about an independent study of random imaginary coupling between the fermions and bosons by Wang [95]. Because of the difference in the fermion-boson coupling, pairing occurs at higher order in the expansion in $1/N$. However, our normal-state results agree with those of Ref. [95].

ACKNOWLEDGMENTS

We are grateful to D. Bagrets, E. Berg, A. L. Chudnovskiy, J. C. Seamus Davis, S. A. Hartnoll, A. Kamenev, Y. Wang, and in particular A. V. Chubukov, S. A. Kivelson, K. Schalm, and Y. Schattner for stimulating discussions. J.S. was funded by the Gordon and Betty Moore Foundation's EPiQS Initiative through Grant No. GBMF4302 while visiting the Geballe Laboratory for Advanced Materials at Stanford University. I.E. was supported by NSF Grant No. DMR-1608055 at Stanford. We are grateful to Y. Wang for sharing his unpublished work with us.

APPENDIX A: DERIVATION OF THE SELF-CONSISTENCY EQUATIONS

After performing the disorder average with the help of the replica trick, we obtain for the averaged replicated partition function

$$\overline{Z^n} = \int \mathcal{D}^n c^\dagger \mathcal{D} c \mathcal{D}^n \phi e^{-S}, \tag{A1}$$

where the action is of the form

$$S = S_0 + S_g. \tag{A2}$$

The bare action is given as

$$S_0 = \sum_{i\sigma a} \int d\tau\, c^\dagger_{i\sigma a}(\tau)(\partial_\tau - \mu) c_{i\sigma a}(\tau) + \sum_{ia} \int d\tau\, \phi_{ia}(\tau)\big(-\partial_\tau^2 + m_0\big)\phi_{ia}(\tau), \tag{A3}$$

while the disorder-average induced interaction term is

$$S_g = -\frac{g^2}{4N^2} \sum_{ijk} \left(\sum_{a\sigma} \int d\tau\, c^\dagger_{i\sigma a}(\tau) c_{j\sigma a}(\tau)\phi_{ka}(\tau) + \sum_{a\sigma} \int d\tau\, c^\dagger_{j\sigma a}(\tau) c_{i\sigma a}(\tau)\phi_{ka}(\tau) \right)^2, \tag{A4}$$

a result that can be rewritten as

$$S_g = \frac{g^2}{2N^2} \sum_{ab\sigma\sigma'} \int d\tau\, d\tau' \sum_i^N \phi_{ia}(\tau)\phi_{ib}(\tau') \times \left[\sum_i^N c^\dagger_{i\sigma a}(\tau) c_{i\sigma' b}(\tau') \sum_j^N c^\dagger_{j\sigma' b}(\tau') c_{j\sigma a}(\tau) - \left(\sum_i^N c^\dagger_{i\sigma a}(\tau) c^\dagger_{i\sigma' b}(\tau') \right) \left(\sum_j^N c_{j\sigma' b}(\tau') c_{j\sigma a}(\tau) \right) \right]. \tag{A5}$$

In order to analyze the action, we introduce collective variables $G(\tau, \tau')$ and Lagrange multiplyer fields $\Sigma(\tau, \tau)$

$$1 = \int \mathcal{D}G \prod_{ab\tau\tau'} \delta\left(N G_{ba,\sigma'\sigma}(\tau', \tau) - \sum_i c^\dagger_{i\sigma a}(\tau) c_{i\sigma' b}(\tau') \right) = \int \mathcal{D}G\, \mathcal{D}\Sigma\, e^{\sum_{ab,\sigma\sigma'} \int d\tau\, d\tau' [N G_{ba,\sigma'\sigma}(\tau',\tau) - \sum_i c^\dagger_{i\sigma a}(\tau) c_{i\sigma' b}(\tau')]} \times \Sigma_{ab,\sigma\sigma'}(\tau, \tau'), \tag{A6}$$

that allow for an efficient decoupling of the interaction terms. Because of the last term in S_g we also include corresponding

anomalous propagators and self-energies:

$$1 = \int \mathcal{D}F \prod_{ab\tau\tau'} \delta\left(NF_{ba,\sigma'\sigma}(\tau',\tau) - \sum_i c_{i\sigma a}(\tau)c_{i\sigma' b}(\tau')\right) = \int \mathcal{D}F\, \mathcal{D}\Phi^+ e^{\sum_{ab,\sigma\sigma'} \int d\tau d\tau' [NF_{ba,\sigma'\sigma}(\tau',\tau) - \sum_i c_{i\sigma a}(\tau)c_{i\sigma' b}(\tau')]\Phi^+_{ab,\sigma\sigma'}(\tau,\tau')}, \tag{A7}$$

as well as

$$\begin{aligned} 1 &= \int \mathcal{D}F^+ \prod_{ab\tau\tau'} \delta\left(NF^+_{ba,\sigma'\sigma}(\tau',\tau) - \sum_i c^\dagger_{i\sigma a}(\tau)c^\dagger_{i\sigma' b}(\tau')\right) \\ &= \int \mathcal{D}F^+ \mathcal{D}\Phi\, e^{\sum_{ab,\sigma\sigma'} \int d\tau d\tau' [NF^+_{ba,\sigma'\sigma}(\tau',\tau) - \sum_i c^\dagger_{i\sigma a}(\tau)c^\dagger_{i\sigma' b}(\tau')]\Phi_{ab,\sigma\sigma'}(\tau,\tau')}. \end{aligned} \tag{A8}$$

Finally, for the bosonic degrees of freedom we use

$$1 = \int \mathcal{D}D \prod_{ab\tau\tau'} \delta\left(ND_{ab}(\tau,\tau') - \sum_i \phi_{ia}(\tau)\phi_{ib}(\tau')\right) = \int \mathcal{D}D\, \mathcal{D}\Pi\, e^{\frac{1}{2}\sum_{ab} \int d\tau\, d\tau' [ND_{ba}(\tau',\tau) - \sum_i \phi_{ia}(\tau)\phi_{ib}(\tau')]\Pi_{ab}(\tau,\tau')}$$

and obtain an effective action with a sizable amount of integration variables:

$$\overline{Z^n} = \int \mathcal{D}G\, \mathcal{D}\Sigma\, \mathcal{D}F^+ \mathcal{D}\Phi^+ \mathcal{D}F\, \mathcal{D}\Phi\, \mathcal{D}D\, \mathcal{D}\Pi\, \mathcal{D}^n c^\dagger \mathcal{D}^n c \mathcal{D}\phi e^{-S},$$

where the collective action is now given as

$$\begin{aligned} S = &\sum_{iab\sigma\sigma'} \int d\tau\, d\tau' c^\dagger_{i\sigma a}(\tau)[(\partial_\tau - \mu)\delta_{ab}\delta_{\sigma\sigma'}\delta(\tau-\tau') + \Sigma_{ab,\sigma\sigma'}(\tau,\tau')]c_{i\sigma' b}(\tau') \\ &+ \sum_{iab\sigma\sigma'} \int d\tau\, d\tau' [c^\dagger_{i\sigma a}(\tau)\Phi_{ab,\sigma\sigma'}(\tau,\tau')c^\dagger_{i\sigma' b}(\tau') + c_{i\sigma a}(\tau)\Phi^+_{ab,\sigma\sigma'}(\tau,\tau')c_{i\sigma' b}(\tau')] \qquad \text{(A9)} \\ &+ \frac{1}{2}\sum_{iab} \int d\tau\, d\tau' \phi_{ia}(\tau)\left[\left(-\partial_\tau^2 + m\right)\delta_{ab}\delta(\tau-\tau') - \Pi_{ab}(\tau,\tau')\right]\phi_{ib}(\tau') \\ &- N\sum_{ab,\sigma\sigma'} \int d\tau\, d\tau' G_{ba,\sigma'\sigma}(\tau',\tau)\Sigma_{ab\sigma\sigma'}(\tau,\tau') + \frac{N}{2}\sum_{ab} \int d\tau\, d\tau' D_{ba}(\tau',\tau)\Pi_{ab}(\tau,\tau') \\ &- N\sum_{ab,\sigma\sigma'} \int d\tau\, d\tau' F_{ba,\sigma'\sigma}(\tau',\tau)\Phi_{ab\sigma\sigma'}(\tau,\tau') - N\sum_{ab,\sigma\sigma'} \int d\tau\, d\tau' F^+_{ba,\sigma'\sigma}(\tau',\tau)\Phi^+_{ab\sigma\sigma'}(\tau,\tau') \\ &+ N\frac{g^2}{2}\sum_{ab\sigma\sigma'} \int d\tau\, d\tau' (G_{ab,\sigma\sigma'}(\tau,\tau')G_{ba,\sigma'\sigma}(\tau',\tau) - F^+_{ab,\sigma\sigma'}(\tau,\tau')F_{ba,\sigma'\sigma}(\tau',\tau))D_{ab}(\tau,\tau'). \qquad \text{(A10)} \end{aligned}$$

We use the Nambu spinor

$$\psi_{ia}(\tau) = (c_{i\uparrow a}(\tau), c_{i\downarrow a}(\tau), c^\dagger_{i\uparrow a}(\tau), c^\dagger_{i\downarrow a}(\tau))^T$$

and rewrite the first two lines of the previous equation as

$$S_{\text{ferm}} = -\frac{1}{2}\sum_{iab} \int d\tau\, d\tau' \psi^\dagger_{ia}(\tau) \begin{pmatrix} G^{-1}_{0,ab}(\tau,\tau') - \Sigma_{ab}(\tau,\tau') & \Phi_{ab}(\tau,\tau') \\ \Phi^+_{ab}(\tau,\tau') & -G^{-1}_{0,ba}(\tau',\tau) + \Sigma_{ba}(\tau',\tau) \end{pmatrix} \psi_{ib}(\tau').$$

Here, we introduced the bare propagator

$$G^{-1}_{0,ab}(\tau,\tau') = -(\partial_\tau - \mu)\delta_{ab}\sigma_0\delta(\tau-\tau'),$$

where σ_0 is the 2×2 identity matrix. Then, we can work with matrices in Nambu space

$$\hat{G}^{-1}_{0,ab}(\tau,\tau') = \begin{pmatrix} G^{-1}_{0,ab}(\tau,\tau') & 0 \\ 0 & -G^{-1}_{0,ba}(\tau',\tau) \end{pmatrix} \tag{A11}$$

and

$$\hat{\Sigma}_{ab}(\tau,\tau') = \begin{pmatrix} \Sigma_{ab}(\tau,\tau') & \Phi_{ab}(\tau,\tau') \\ \Phi^{+}_{ab}(\tau,\tau') & -\Sigma_{ba}(\tau',\tau) \end{pmatrix}. \tag{A12}$$

Here, $\Sigma_{ab}(\tau,\tau')$ and $\Phi_{ab}(\tau,\tau')$, etc., are still 2×2 matrices in spin space. In addition we use for the bare phonon propagator

$$D_0^{-1}(\tau,\tau') = \left(-\partial_\tau^2 + m\right)\delta(\tau-\tau'). \tag{A13}$$

We can now integrate out the fermions and bosons:

$$\begin{aligned} S = &-N\,\mathrm{tr}\,\log\left(\hat{G}_0^{-1} - \hat{\Sigma}\right) + \frac{N}{2}\mathrm{tr}\,\log\left(D_0^{-1}(\tau,\tau')\delta_{ab} - \Pi_{ab}(\tau,\tau')\right) \\ &- N\sum_{ab,\sigma\sigma'}\int d\tau\, d\tau' G_{ba,\sigma'\sigma}(\tau',\tau)\Sigma_{ab\sigma\sigma'}(\tau,\tau') + \frac{N}{2}\sum_{ab}\int d\tau\, d\tau' D_{ba}(\tau',\tau)\Pi_{ab}(\tau,\tau') \\ &- N\sum_{ab,\sigma\sigma'}\int d\tau\, d\tau' F_{ba,\sigma'\sigma}(\tau',\tau)\Phi_{ab\sigma\sigma'}(\tau,\tau') - N\sum_{ab,\sigma\sigma'}\int d\tau\, d\tau' F^{+}_{ba,\sigma'\sigma}(\tau',\tau)\Phi^{+}_{ab\sigma\sigma'}(\tau,\tau') \\ &+ N\frac{g^2}{2}\sum_{ab\sigma\sigma'}\int d\tau\, d\tau'\left(G_{ab,\sigma\sigma'}(\tau,\tau')G_{ba,\sigma'\sigma}(\tau',\tau) - F^{+}_{ab,\sigma\sigma'}(\tau,\tau')F_{ba,\sigma'\sigma}(\tau',\tau)\right)D_{ab}(\tau,\tau'). \end{aligned} \tag{A14}$$

We assume a replica-diagonal structure such that $\overline{Z^n} = \overline{Z}^n$. Thus, the average is essentially an annealed one. Now, the replica structure disappears from the action that determines $\overline{Z}$:

$$\begin{aligned} S = &-N\,\mathrm{tr}\,\log\left(\hat{G}_0^{-1} - \hat{\Sigma}\right) + \frac{N}{2}\mathrm{tr}\,\log\left(D_0^{-1} - \Pi\right) - N\sum_{\sigma\sigma'}\int d\tau\, d\tau' G_{\sigma'\sigma}(\tau',\tau)\Sigma_{\sigma\sigma'}(\tau,\tau') + \frac{N}{2}\int d\tau\, d\tau' D(\tau',\tau)\Pi(\tau,\tau') \\ &- N\sum_{\sigma\sigma'}\int d\tau\, d\tau' F_{\sigma'\sigma}(\tau',\tau)\Phi^{+}_{\sigma\sigma'}(\tau,\tau') - N\sum_{\sigma\sigma'}\int d\tau\, d\tau' F^{+}_{\sigma'\sigma}(\tau',\tau)\Phi_{\sigma\sigma'}(\tau,\tau') \\ &+ N\frac{g^2}{2}\sum_{\sigma\sigma'}\int d\tau\, d\tau'\left(G_{\sigma\sigma'}(\tau,\tau')G_{\sigma'\sigma}(\tau',\tau) - F^{+}_{\sigma\sigma'}(\tau,\tau')F_{\sigma'\sigma}(\tau',\tau)\right)D(\tau,\tau'). \end{aligned} \tag{A15}$$

At large N we can perform the saddle-point approximation and obtain the stationary equations

$$\begin{aligned} &G(\tau,\tau') = \left(G_0^{-1} - \Sigma\right)^{-1}_{\tau,\tau'}, \quad D(\tau,\tau') = \left(D_0^{-1} - \Pi\right)^{-1}_{\tau,\tau'}, \quad \Sigma_{\sigma\sigma'}(\tau,\tau') = g^2 G_{\sigma\sigma'}(\tau,\tau')D(\tau,\tau'), \\ &\Phi_{\sigma\sigma'}(\tau,\tau') = -g^2 F_{\sigma\sigma'}(\tau',\tau)D(\tau,\tau'), \quad \Pi(\tau,\tau') = -g^2\sum_{\sigma\sigma'}\left(G_{\sigma\sigma'}(\tau',\tau)G_{\sigma'\sigma}(\tau,\tau') - F^{+}_{\sigma\sigma'}(\tau',\tau)F_{\sigma\sigma'}(\tau,\tau')\right). \end{aligned} \tag{A16}$$

If we focus on singlet pairing we have $F_{\sigma\sigma'}(\tau) = F(\tau)i\sigma^{y}_{\sigma\sigma'}$ and $F^{+}_{\sigma\sigma'}(\tau) = -F^{+}(\tau)i\sigma^{y}_{\sigma\sigma'}$. Now, we can rewrite these equations in the usual fashion in 2×2 Nambu space with $(c_{i\uparrow}, c^{\dagger}_{i\downarrow})$ with fermionic Green's function

$$\hat{G}(\omega_n)^{-1} = i\omega_n\tau_0 + \mu\tau_3 - \hat{\Sigma}(\omega_n). \tag{A17}$$

For the bosons we use

$$D(\nu_n) = \frac{1}{\nu_n^2 + \omega_0^2 + \Pi(\nu_n)}. \tag{A18}$$

Then, the self-energies are given as

$$\begin{aligned} &\hat{\Sigma}(\tau) = g^2\tau_3\hat{G}(\tau)\tau_3 D(\tau), \\ &\Pi(\tau) = -g^2\mathrm{tr}(\tau_3\hat{G}(\tau)\tau_3\hat{G}(-\tau)). \end{aligned} \tag{A19}$$

Those are the coupled equations given above.

APPENDIX B: DERIVATION OF THE NORMAL-STATE RESULTS

In this Appendix we summarize the derivation of the electron and phonon propagators for the two normal-state regimes. We start our analysis with the behavior in the low-temperature quantum-critical SYK regime and continue with the intermediate-temperature impuritylike behavior at strong coupling. In addition to the analytic derivation, we also present results of the full numerical solution that confirm our analytic findings in detail.

1. Quantum-critical SYK fixed point: Derivation of Eqs. (16)–(18) and numerical results

We start our analysis at $T = 0$ and make the following ansatz for the fermionic self-energy:

$$\Sigma(\omega) = -i\lambda\,\mathrm{sign}(\omega)|\omega|^{1-2\Delta}. \tag{B1}$$

To preserve causality, the coefficient λ has to be positive. This is most transparent if one analytically continues this ansatz to the real frequency axis. Here, causality requires that the retarded self-energy has a negative imaginary part. With $\mathrm{Im}\,\Sigma^{R}(\epsilon) = -\sin(\pi\Delta)\lambda|\epsilon|^{\eta}$ follows $\lambda > 0$ for $0 < \Delta < 1$.

As long as $\Delta > 0$, the low-energy fermionic Green's function is dominated by this singular self-energy

$$G(\omega) \approx -\frac{1}{\Sigma(\omega)} = -\frac{i}{\lambda}\text{sign}(\omega)|\omega|^{-(1-2\Delta)}. \tag{B2}$$

On the real axis this corresponds to the spectral function $A(\epsilon) = -\frac{1}{\pi}\text{Im}G^R(\epsilon) = \frac{\sin(\pi\Delta)|\epsilon|^{-(1-2\Delta)}}{\lambda\pi}$. The bosonic self-energy is

$$\begin{aligned}\Pi(\omega) &= -2\bar{g}^2\int\frac{d\omega}{2\pi}G(\omega)G(\omega+\Omega)\\ &= \frac{2g^2}{\lambda^2}\int\frac{d\omega}{2\pi}\frac{\text{sign}(\omega)\text{sign}(\omega+\Omega)}{|\omega|^{1-2\Delta}|\omega+\Omega|^{1-2\Delta}}.\end{aligned} \tag{B3}$$

This bosonic self-energy for $\Omega \to 0$ is ultraviolet divergent if $\Delta > \frac{1}{4}$, i.e., $\Pi(0) \propto \Lambda^{4\Delta-1}$ with upper cutoff Λ. This divergence can be avoided if we include the full propagator and write

$$\begin{aligned}\Pi(0) &= -2\bar{g}^2\int\frac{d\omega}{2\pi}G(\omega)^2 = -2g^2\int\frac{d\omega}{2\pi}\left(\frac{1}{i\omega-\Sigma(\omega)}\right)^2\\ &= \frac{2\Delta-1}{2\Delta^2\sin\frac{\pi}{2\Delta}}\bar{g}^2\lambda^{-\frac{1}{2\Delta}}.\end{aligned} \tag{B4}$$

Next, we analyze the dynamic part $\delta\Pi(\omega) = \Pi(\omega) - \Pi(0)$. It is easiest to do this by first Fourier transforming the propagator to imaginary time:

$$G(\tau) = -\frac{\Gamma(2\Delta)\sin(\pi\Delta)}{\pi\lambda}\frac{\text{sign}(\tau)}{|\tau|^{2\Delta}}, \tag{B5}$$

such that the Fourier transform of the phonon self-energy is given as $\Pi(\tau) = 2g^2(\frac{\Gamma(2\Delta)\sin(\pi\Delta)}{\pi\lambda})^2\frac{1}{|\tau|^{4\Delta}}$, which yields

$$\begin{aligned}\delta\Pi(\omega) &= 2\int_0^\infty\Pi(\tau)[\cos(\omega\tau)-1]d\tau\\ &= -\frac{g^2}{\lambda^2}C_\Delta|\omega|^{4\Delta-1}\end{aligned}$$

with coefficient $C_\Delta = -8\cos(\pi\Delta)\sin^3(\pi\Delta)\Gamma(2\Delta)^2\Gamma(1-4\Delta)/\pi^2$.

Now, we can analyze the bosonic propagator $D(\omega)$. We can neglect the bare Ω^2 term against the singular bosonic frequency dependence due to the Landau damping. In addition, we can only expect a power-law solution if indeed $\omega_0^2 - \Pi(0) = 0$. If this is the case, it follows for the bosonic propagator

$$D(\omega) \approx -\frac{1}{\delta\Pi(\omega)} = \frac{\lambda^2}{\bar{g}^2C_\Delta}|\Omega|^{1-4\Delta}. \tag{B6}$$

The Fourier transform is $D(\tau) = \frac{\lambda^2}{g^2}B_\Delta\frac{1}{|\tau|^{2-4\Delta}}$ with $B_\Delta = \frac{\pi(1-4\Delta)\cos(2\pi\Delta)}{8\Gamma(2\Delta)^2\cos(\pi\Delta)\sin^3(\pi\Delta)}$ which gives for the self-energy

$$\Sigma(\tau) = -\lambda\frac{B_\Delta\Gamma(2\Delta)\sin(\pi\Delta)}{\pi}\frac{\text{sign}(\tau)}{|\tau|^{2-2\Delta}}. \tag{B7}$$

Fourier transforming this back to the Matsubara frequency axis finally yields

$$\Sigma(\omega) = -i\lambda A_\Delta\text{sign}(\omega)|\omega|^{1-2\Delta} \tag{B8}$$

with

$$A_\Delta = \frac{4\Delta-1}{2(2\Delta-1)[\sec(2\pi\Delta)-1]}. \tag{B9}$$

Notice, for the Fourier transforms to be well defined, it must hold that $\frac{1}{4} < \Delta < \frac{1}{2}$. In order to have a self-consistent solution it must of course hold that $A_\Delta = 1$. This determines the exponent Δ given in Eq. (19). Interestingly, the coefficient λ remains undetermined by this procedure. However, our solution still relies on the assumption that the renormalized phonon frequency vanishes at $T = 0$. We have not yet determined when this is the case. We can now always use the freedom and determine λ such that $\omega_r(T=0) = 0$, which yields the condition

$$\lambda = c_1 g^{4\Delta} \tag{B10}$$

in order to generate a critical state for all values of the coupling constant. The numerical coefficient is

$$c_1 = \left(\frac{2\Delta-1}{2\Delta^2\sin\frac{\pi}{2\Delta}}\right)^{2\Delta}. \tag{B11}$$

With Δ from Eq. (19) follows $c_1 \approx 0.832\,260\,211\,4$. There is one caveat in this argumentation. The relationship between $\Pi(0)$ and λ that we used to determine the coefficient c_1 relied on the simultaneous knowledge of the low- and high-frequency behaviors of the fermionic propagator [see Eq. (B4)]. To address this, we used an expression that interpolates between the two known limits. Such an approach gives the correct qualitative behavior. Yet, the numerical value for c_1 cannot be reliably determined by such a procedure. To avoid this uncertainty we determine this coefficient from the full numerical solution of the problem that confirms our scaling results in detail; see below. This yields $c_1 \approx 1.154\,700\,5$ which is somewhat larger than the above estimate. In what follows we will use this result for c_1. Notice, all other coefficients of our analysis, such as C_Δ or A_Δ, can be uniquely determined by the universal low-energy behavior and do not have to be determined numerically.

These results for the phonon frequency allow us to determine the coefficient of the dynamic part of the boson propagator

$$\delta\Pi(\omega) = -c_3\left|\frac{\omega}{g^2}\right|^{4\Delta-1}, \tag{B12}$$

where $c_3 = \frac{C_\Delta}{c_1^2}$. With Δ from Eq. (19) and the numerically determined value of c_1 follows $c_3 \approx 0.709\,618$.

This analysis further allows us to determine the temperature dependence of the phonon frequency, which is determined via

$$\omega_r^2(T) = \omega_0^2 - \Pi(T), \tag{B13}$$

where

$$\Pi(T) = -2g^2T\sum_{n=-\infty}^{\infty}G(\omega_n)^2. \tag{B14}$$

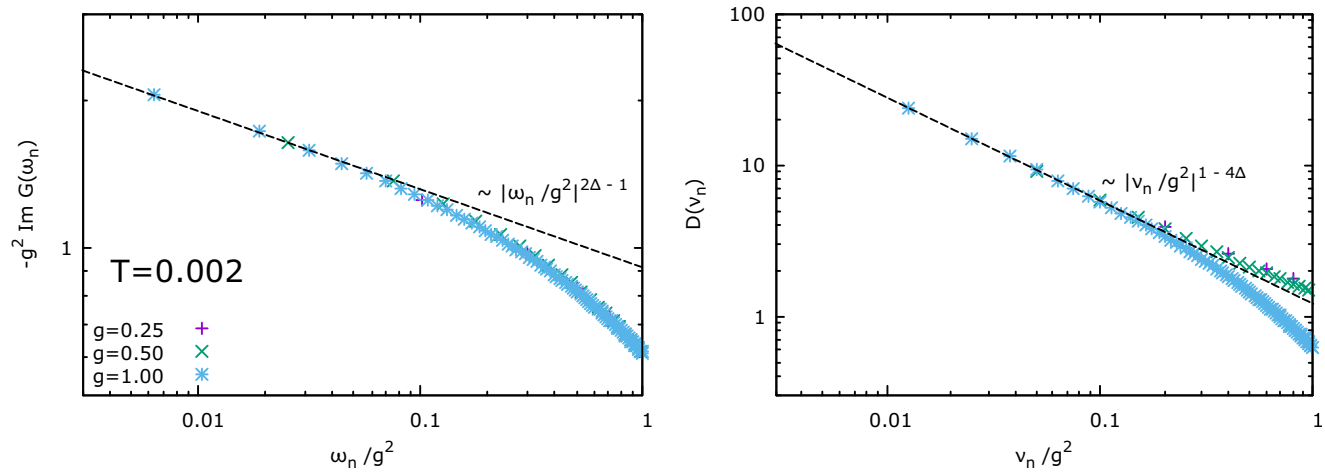

FIG. 12. Numerical solution of the fermionic (left panel) and bosonic (right panel) propagators on the imaginary axis in comparison with the analytic solution given in Eqs. (16) and (17).

At low but finite temperatures we use for the propagator our result

$$G(\omega_n) = \frac{1}{i\omega_n + i\lambda\,\mathrm{sign}(\omega_n)|\omega_n|^{1-2\Delta}}. \tag{B15}$$

Using the Poisson summation formula for fermionic Matsubara sums gives for the phonon frequency

$$\omega_r^2(T) = \omega_0^2 - 2g^2 \sum_{k=-\infty}^{\infty} (-1)^k \int_0^{\infty} \frac{d\omega}{\pi} \frac{\cos(\beta\omega k)}{(\omega + \lambda\omega^{1-2\Delta})^2}. \tag{B16}$$

The $k = 0$ term corresponds to the $T = 0$ result. Thus, it exactly cancels the bare frequency. The remaining frequency integrals are ultraviolet convergent even without the bare fermionic propagator included, which finally gives

$$\omega_r^2(T) = \frac{4g^2}{\lambda^2} \sum_{k=1}^{\infty} (-1)^{k+1} \int_0^{\infty} \frac{d\omega}{\pi} \frac{\cos(\beta\omega k)}{\omega^{2-4\Delta}} = c_2 \left(\frac{T}{g^2}\right)^{4\Delta-1}, \tag{B17}$$

with numerical coefficient

$$c_2 = \frac{4}{\pi c_1^2} \sin(2\pi\Delta)\Gamma(4\Delta - 1)(1 - 2^{2-4\Delta})\zeta(4\Delta - 1), \tag{B18}$$

where c_1 was determined numerically [see text below Eq. (B11)]. With Δ from Eq. (19) follows $c_2 \approx 0.561\,228$.

We finish this discussion with a comparison of our analytical results with the numerical solutions of the coupled equations in the normal state. In Fig. 12 we compare the fermionic and bosonic propagators as function of the imaginary Matsubara frequency with our analytic solution of Eqs. (16) and (17). Finally, in Fig. 13 we demonstrate that the phonon frequency agrees with our analytical result (18). In particular, this demonstrates that indeed the phonon frequency is soft for all values of g.

2. Impuritylike fixed point: Derivation of Eqs. (23)–(25) and numerical results

Let us assume that the boson propagator behaves as in Eq. (24) with renormalized boson frequency ω_r, but without additional dynamic renormalizations due to Landau damping. We further assume $T \gg \omega_r$ something we need to check below to be consistent. Then it follows that the self-energy is dominated by the lowest bosonic Matsubara frequency, i.e., bosons behave as classical impurities:

$$\Sigma(\omega_n) = g^2 T \sum_{n'} D(\omega_n - \omega_{n'})G(\omega_{n'}) = \frac{g^2 T}{\omega_r^2} \frac{1}{i\omega_n - \Sigma(\omega_n)}. \tag{B19}$$

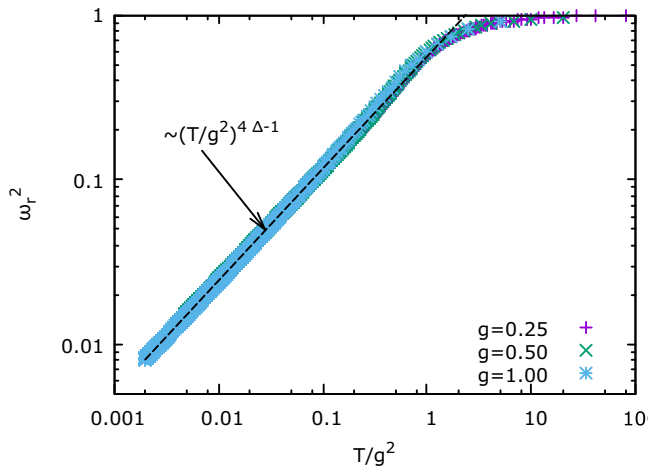

FIG. 13. Temperature dependence of the renormalized phonon frequency for several values of the coupling constant g determined from the numerical solution of the coupled equations and compared with the analytical expression of Eq. (18).

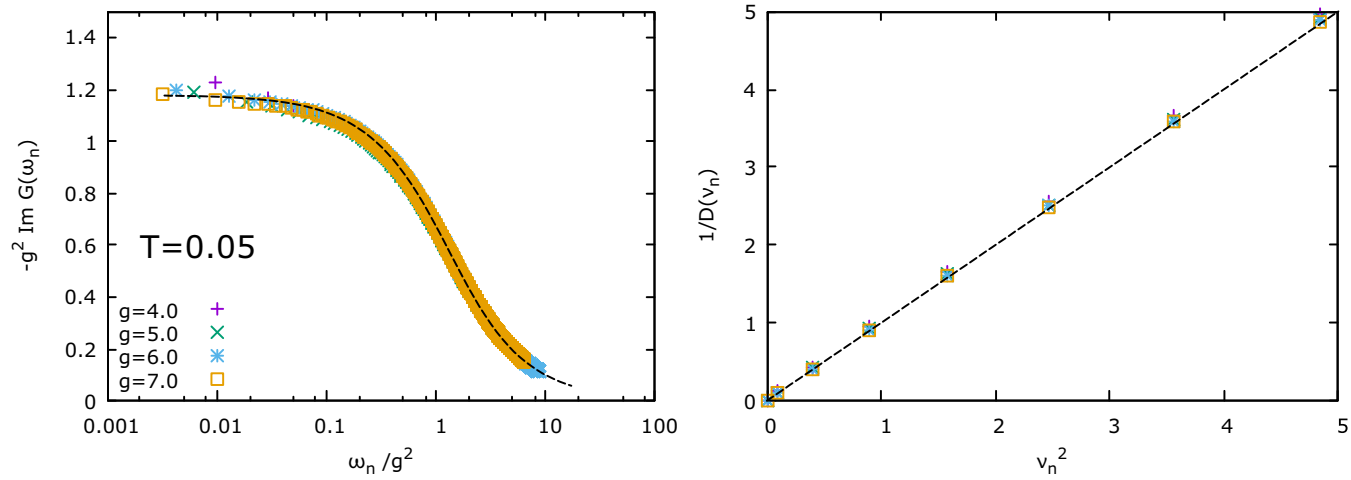

FIG. 14. Numerical solution of the fermionic (left panel) and bosonic (right panel) propagators on the imaginary axis in comparison with the analytic solution given in Eqs. (23) and (24).

This suggests to introduce the energy scale $\Omega_0 = 2\sqrt{\frac{g^2 T}{\omega_r^2}}$ which yields

$$\Sigma(\omega_n) = -i\,\mathrm{sign}(\omega_n)\tfrac{1}{2}\left(\sqrt{\omega_n^2+\Omega_0^2} - |\omega_n|\right) \tag{B20}$$

as the solution of the above quadratic equation. For $|\omega_n| \ll \Omega_0$ holds $\Sigma(\omega_n) = -i\,\mathrm{sign}(\omega_n)\frac{\Omega_0}{2}$ while for large frequencies it follows that $\Sigma(\omega_n) = -i\,\mathrm{sign}(\omega_n)\frac{\Omega_0^2}{4|\omega|}$. For the fermionic Green's function follows then Eq. (23). Next, we determine the bosonic self-energy for this problem:

$$\Pi(\omega_n) = -2g^2 T \sum_{n'} G(\omega_{n'}) G(\omega_{n'} + \omega_n). \tag{B21}$$

Let us first determine the zero-frequency part

$$\begin{aligned}\Pi(0) &= -2g^2 T \sum_{n'} G(\omega_{n'})^2 \\ &= 8g^2 T \sum_{n'} \frac{1}{\left(\sqrt{\omega_n^2+\Omega_0^2} + |\omega_n|\right)^2}.\end{aligned} \tag{B22}$$

Let us try to determine Ω_0 from the condition that the boson frequency goes to zero as T is extrapolated to $T = 0$. Formally we can just require that $\Pi(0) = \omega_0^2$ at $T = 0$. Then, we have

$$\begin{aligned}\Pi(0) &= 8g^2 \int_0^\infty \frac{d\omega}{\pi} \frac{1}{\left(\sqrt{\omega^2+\Omega_0^2} + \omega\right)^2} \\ &= \frac{16 g^2}{3\pi\,\Omega_0}.\end{aligned} \tag{B23}$$

This yields $\Omega_0 = \frac{16}{3\pi} g^2$. Combining both expressions that we obtained for Ω_0 can be used to determine the phonon frequency and gives rise to our result (25). The assumption of classical bosons was $T \gg \omega_r$ which implies $T \gg g^{-2}$, consistent in the strong-coupling limit. In addition, as long as $T \ll g^2$ we also have $T \ll \Omega_0$ and the evaluation of the above fermionic Matsubara sum in the zero-temperature limit is justified. The frequency dependence of the self-energy for $\omega \ll g^2$ is then $\Sigma(\omega_n) = -i\,\mathrm{sign}(\omega_n)\frac{8}{3\pi} g^2$.

For consistency we have to check that we can indeed ignore the frequency dependence of the bosonic self-energy. The only scale that enters the fermionic propagator is Ω_0. In the relevant limit $T \ll \Omega_0$ the fermions are essentially at zero temperature, where

$$\begin{aligned}\delta\Pi(\omega) &= 2\int_0^\infty d\tau\, \Pi(\tau)[\cos(\omega\tau) - 1] \\ &= -4g^2 \int_0^\infty d\tau\, G(\tau) G(-\tau)[\cos(\omega\tau) - 1].\end{aligned}$$

The Fourier transform of the fermionic propagator can be determined analytically and expressed in terms of modified Bessel functions and the modified Struve function. For our

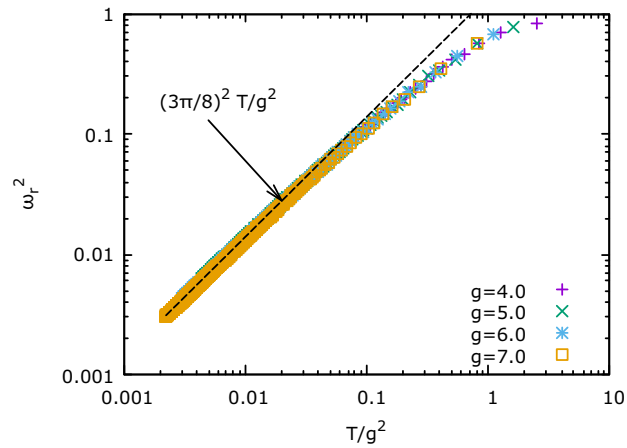

FIG. 15. Temperature dependence of the renormalized phonon frequency for several values of the coupling constant g determined from the numerical solution of the coupled equations and compared with the analytical expression of Eq. (25).

purposes it suffices to analyze the short- and long-time limits:

$$G(\tau) = \mathrm{sign}(\tau) \times \begin{cases} \frac{1}{\Omega_0|\tau|} & \text{if } |\tau| \gg \Omega_0^{-1}, \\ \frac{1}{2} - \frac{2}{3\pi}|\tau|\Omega_0 & \text{if } |\tau| \ll \Omega_0^{-1}, \end{cases} \quad \text{(B24)}$$

which yields

$$\delta\Pi(\omega) \approx -\frac{|\omega|}{\Omega_0}.$$

This Landau damping term is negligible compared to ω_n^2 for $T \gg g^{-2}$. Thus, we can indeed approximate the bosonic propagator by Eq. (24).

We finish this discussion with a comparison of our analytical results with the numerical solutions of the coupled equations in the normal state. In Fig. 14 we compare the fermionic and bosonic propagators as function of the imaginary Matsubara frequency with our analytic solution of Eqs. (23) and (24). Finally, in Fig. 15 we demonstrate that the phonon frequency agrees with our analytical result (25).

APPENDIX C: ON THE ROLE OF DISTINCT FERMION AND BOSON MODES

The ratio $m = M/N$ changes the relative importance of the fermion and boson self-energies. Changing the ratio m of the number of boson and fermion flavors does not affect the overall behavior of Eqs. (10) and (17). The exponent Δ changes continuously from $\Delta(m \to 0) \to 1/2$ to $\Delta(m \to \infty) \to 1/4$. The phonon softening still formally follows Eq. (18), yet the temperature scale below which this power-law softening occurs depends sensitively on the relative importance of the phonon and electron renormalizations. If phonon self-energy effects dominate ($m \ll 1$) we find $\omega_r^2 = \frac{m}{4}\pi^2 \log 2(T/g^2)^{1-\frac{m}{2}}$, i.e., phonons are soft below a very large temperature $T^* \sim g^2/m^{1-\frac{m}{2}}$. In the opposite limit, of large m, i.e., relatively negligible phonon self-energy, $\omega_r^2 \approx (\frac{T}{g^2})^{\sqrt{\frac{2}{\pi m}}}$ and the temperature window below which phonon softening takes place is exponentially small $T^* \sim g^2 e^{-\sqrt{\frac{\pi m}{2}}}$.

[1] L. N. Cooper, Bound electron pairs in a degenerate Fermi gas, Phys. Rev. **104**, 1189 (1956).

[2] J. Bardeen, L. N. Cooper, and J. R. Schrieffer, Microscopic theory of superconductivity, Phys. Rev. **106**, 162 (1957).

[3] J. Bardeen, L. N. Cooper, and J. R. Schrieffer, Theory of superconductivity, Phys. Rev. **108**, 1175 (1957).

[4] W. Kohn and J. M. Luttinger, New Mechanism for Superconductivity, Phys. Rev. Lett. **15**, 524 (1965).

[5] D. S. Dessau, B. O. Wells, Z.-X. Shen, W. E. Spicer, A. J. Arko, R. S. List, D. B. Mitzi, and A. Kapitulnik, Anomalous Spectral Weight Transfer at the Superconducting Transition of $Bi_2Sr_2CaCu_2O_{8+\delta}$, Phys. Rev. Lett. **66**, 2160 (1991).

[6] Z.-X. Shen and J. R. Schrieffer, Momentum, Temperature, and Doping Dependence of Photoemission Lineshape and Implications for the Nature of the Pairing Potential in High-T_c Superconducting Materials, Phys. Rev. Lett. **78**, 1771 (1997).

[7] J. C. Campuzano, H. Ding, M. R. Norman, M. Randeira, A. F. Bellman, T. Yokoya, T. Takahashi, H. Katayama-Yoshida, T. Mochiku, and K. Kadowaki, Direct observation of particle-hole mixing in the superconducting state by angle-resolved photoemission, Phys. Rev. B **53**, R14737(R) (1996).

[8] A. V. Fedorov, T. Valla, P. D. Johnson, Q. Li, G. D. Gu, and N. Koshizuka, Temperature Dependent Photoemission Studies of Optimally Doped $Bi_2Sr_2CaCu_2O_8$, Phys. Rev. Lett. **82**, 2179 (1999).

[9] D. L. Feng, D. H. Lu, K. M. Shen, C. Kim, H. Eisaki, A. Damascelli, R. Yoshizaki, J.-i. Shimoyama, K. Kishio, G. D. Gu, S. Oh, A. Andrus, J. O'Donnell, J. N. Eckstein, and Z.-X. Shen, Signature of superfluid density in the single-particle excitation spectrum of $Bi_2Sr_2CaCu_2O_{8+\delta}$, Science **289**, 277 (2000).

[10] A. Balatsky, Superconducting instability in a non-Fermi liquid scaling approach, Philos. Mag. Lett. **68**, 251 (1993).

[11] A. Sudbo, Pair Susceptibilities and Gap Equations in Non-Fermi Liquids, Phys. Rev. Lett. **74**, 2575 (1995).

[12] L. Yin and S. Chakravarty, Spectral anomaly and high temperature superconductors, Int. J. Mod. Phys. B **10**, 805 (1996).

[13] N. E. Bonesteel, I. A. McDonald, and C. Nayak, Gauge Fields and Pairing in Double-Layer Composite Fermion Metals, Phys. Rev. Lett. **77**, 3009 (1996).

[14] D. T. Son, Superconductivity by long-range color magnetic interaction in high-density quark matter, Phys. Rev. D **59**, 094019 (1999).

[15] Ar. Abanov, A. Chubukov, and A. Finkel'stein, Coherent vs. incoherent pairing in 2D systems near magnetic instability, Europhys. Lett. **54**, 488 (2001).

[16] Ar. Abanov, A. V. Chubukov, and J. Schmalian, Quantum-critical superconductivity in underdoped cuprates, Europhys. Lett. **55**, 369 (2001).

[17] R. Roussev and A. J. Millis, Quantum critical effects on transition temperature of magnetically mediated p-wave superconductivity, Phys. Rev. B **63**, 140504(R) (2001).

[18] A. V. Chubukov and J. Schmalian, Superconductivity due to massless boson exchange in the strong-coupling limit, Phys. Rev. B **72**, 174520 (2005).

[19] J.-H. She and J. Zaanen, BCS superconductivity in quantum critical metals, Phys. Rev. B **80**, 184518 (2009).

[20] E.-G. Moon and A. V. Chubukov, Quantum-critical pairing with varying exponents, Low Temp Phys. **161**, 263 (2010).

[21] M. A. Metlitski, D. F. Mross, S. Sachdev, and T. Senthil, Cooper pairing in non-Fermi liquids, Phys. Rev. B **91**, 115111 (2015).

[22] S. Raghu, G. Torroba, and H. Wang, Metallic quantum critical points with finite BCS couplings, Phys. Rev. B **92**, 205104 (2015).

[23] S. Lederer, Y. Schattner, E. Berg, and S. A. Kivelson, Enhancement of Superconductivity near a Nematic Quantum Critical Point, Phys. Rev. Lett. **114**, 097001 (2015).

[24] Y.-M. Wu, A. Abanov, Y. Wang, and A. V. Chubukov, The special role of the first Matsubara frequency for superconductivity

near a quantum-critical point - the non-linear gap equation below T_c and spectral properties in real frequencies, Phys. Rev. B **99**, 144512 (2019).

[25] A. Abanov, Y.-M. Wu, Y. Wang, and A. V. Chubukov, Superconductivity above a quantum critical point in a metal - gap closing vs gap filling, Fermi arcs, and pseudogap behavior, preprint, Phys. Rev. B **99**, 180506 (2019).

[26] E. Berg, M. A. Metlitski, and S. Sachdev, Sign-problem free quantum monte carlo of the onset of antiferromagnetism in metals, Science **338**, 1606 (2012).

[27] Y. Schattner, M. H. Gerlach, S. Trebst, and E. Berg, Competing Orders in a Nearly Antiferromagnetic Metal, Phys. Rev. Lett. **117**, 097002 (2016).

[28] Y. Schattner, S. Lederer, S. A. Kivelson, and E. Berg, Ising Nematic Quantum Critical Point in a Metal: A Monte Carlo Study, Phys. Rev. X **6**, 031028 (2016).

[29] P. T. Dumitrescu, M. Serbyn, R. T. Scalettar, and A. Vishwanath, Superconductivity and nematic fluctuations in a model of doped FeSe monolayers: Determinant quantum Monte Carlo study, Phys. Rev. B **94**, 155127 (2016).

[30] S. Lederer, Y. Schattner, E. Berg, and S. A. Kivelson, Superconductivity and bad metal behavior near a nematic quantum critical point, Proc. Natl. Acad. Sci. U. S. A. **114**, 4905 (2017).

[31] Z.-X. Li, F. Wang, H. Yao, and D.-H. Lee, Nature of the effective interaction in electron-doped cuprate superconductors: A sign-problem-free quantum Monte Carlo study, Phys. Rev. B **95**, 214505 (2017).

[32] X. Wang, Y. Schattner, E. Berg, and R. M. Fernandes, Superconductivity mediated by quantum critical antiferromagnetic fluctuations: The rise and fall of hot spots, Phys. Rev. B **95**, 174520 (2017).

[33] I. Esterlis, B. Nosarzewski, E. W. Huang, B. Moritz, T. P. Devereaux, D. J. Scalapino, and S. A. Kivelson, Breakdown of the Migdal-Eliashberg theory: A determinant quantum Monte Carlo study, Phys. Rev. B **97**, 140501(R) (2018).

[34] E. Berg, S. Lederer, Y. Schattner, and S. Trebst, Monte Carlo studies of quantum critical metals, Annu. Rev. Condens. Matter Phys. **10**, 63 (2019).

[35] J.-H. She, B. J. Overbosch, Y.-W. Sun, Y. Liu, K. E. Schalm, J. A. Mydosh, and J. Zaanen, Observing the origin of superconductivity in quantum critical metals, Phys. Rev. B **84**, 144527 (2011).

[36] S. Sachdev and J. Ye, Gapless Spin Liquid Ground State in a Random, Quantum Heisenberg Magnet, Phys. Rev. Lett. **70**, 3339 (1993).

[37] A. Georges, O. Parcollet, and S. Sachdev, Mean Field Theory of a Quantum Heisenberg Spin Glass, Phys. Rev. Lett. **85**, 840 (2000).

[38] S. Sachdev, Holographic Metals and the Fractionalized Fermi Liquid, Phys. Rev. Lett. **105**, 151602 (2010).

[39] A. Kitaev, Hidden correlations in the Hawking radiation and thermal noise, Talk at KITP http://online.kitp.ucsb.edu/online/joint98/kitaev/

[40] A. Kitaev, A simple model of quantum holography. Talks at KITP http://online.kitp.ucsb.edu/online/entangled15/kitaev/ and http://online.kitp.ucsb.edu/online/entangled15/kitaev2/

[41] S. Sachdev, Bekenstein-Hawking Entropy and Strange Metals, Phys. Rev. X **5**, 041025(R) (2015).

[42] J. Maldacena and D. Stanford, Remarks on the Sachdev-Ye-Kitaev model, Phys. Rev. D **94**, 106002(R) (2016).

[43] J. Polchinski and V. Rosenhaus, The spectrum in the Sachdev-Ye-Kitaev model, J. High Energy Phys. 04 (2016) 001.

[44] W. Fu, D. Gaiotto, J. Maldacena, and S. Sachdev, Supersymmetric Sachdev-Ye-Kitaev models, Phys. Rev. D **95**, 026009 (2017); Publisher's Note: Supersymmetric Sachdev-Ye-Kitaev models, **95**, 069904(E) (2017).

[45] Z. Bi, C.-M. Jian, Y.-Z. You, K. A. Pawlak, and C. Xu, Instability of the Non-Fermi-liquid state of the Sachdev-Ye-Kitaev model, Phys. Rev. B **95**, 205105 (2017).

[46] X.-Y. Song, C.-M. Jian, and L. Balents, Strongly Correlated Metal Built from Sachdev-Ye-Kitaev Models, Phys. Rev. Lett. **119**, 216601 (2017).

[47] D. Chowdhury, Y. Werman, E. Berg, and T. Senthil, Translationally Invariant Non-Fermi-Liquid Metals with Critical Fermi Surfaces: Solvable Models, Phys. Rev. X **8**, 031024 (2018).

[48] Y. Cao, V. Fatemi, S. Fang, K. Watanabe, T. Taniguchi, E. Kaxiras, and P. Jarillo-Herrero, Unconventional superconductivity in magic-angle graphene superlattices, Nature (London) **556**, 43 (2018).

[49] A. Georges, G. Kotliar, W. Krauth, and M. J. Rozenberg, Dynamical mean-field theory of strongly correlated fermion systems and the limit of infinite dimensions, Rev. Mod. Phys. **68**, 13 (1996).

[50] G. Kotliar, and D. Vollhardt, Strongly correlated materials: Insights from dynamical mean-field theory, Phys. Today **57**(3), 53 (2004).

[51] J. Schmalian and P. Wolynes, Stripe Glasses: Self-Generated Randomness in a Uniformly Frustrated System, Phys. Rev. Lett. **85**, 836 (2000).

[52] H. Westfahl, Jr., J. Schmalian, and P. G. Wolynes, Dynamical mean-field theory of quantum stripe glasses, Phys. Rev. B **68**, 134203 (2003).

[53] D. Bagrets, A. Altland, and A. Kamenev, Sachdev-Ye-Kitaev model as Liouville quantum mechanics, Nucl. Phys. B **911**, 191 (2016).

[54] D. Bagrets, A. Altland, and A. Kamenev, Power-law out of time order correlation functions in the SYK model, Nucl. Phys. B **921**, 727 (2017).

[55] A. A. Patel, M. J. Lawler, and E.-A. Kim, Coherent Superconductivity with a Large Gap Ratio from Incoherent Metals, Phys. Rev. Lett. **121**, 187001 (2018).

[56] N. V. Gnezdilov, Gapless odd-frequency superconductivity induced by the Sachdev-Ye-Kitaev model, Phys. Rev. B **99**, 024506 (2019).

[57] S. A. Hartnoll, C. P. Herzog, and G. T. Horowitz, Building a Holographic Superconductor, Phys. Rev. Lett. **101**, 031601 (2008).

[58] S. A. Hartnoll, C. P. Herzog, and G. T. Horowitz, Holographic superconductors, J. High Energy Phys. 12 (2008) 015.

[59] S. A. Hartnoll, A. Lucas, and S. Sachdev, *Holographic Quantum Matter* (The MIT Press, Cambridge, MA, 2018).

[60] G. M. Eliashberg, Interactions between electrons and lattice vibrations in a superconductor, Zh. Eksp. Teor. Fiz. **38**, 966 (1960) [Sov. Phys.–JETP **11**, 696 (1960)].

[61] D. Scalapino, in *Superconductivity*, edited by R. Parks (CRC Press, Boca Raton, FL, 1969).

[62] J. P. Carbotte, Properties of boson-exchange superconductors, Rev. Mod. Phys. **62**, 1027 (1990).

[63] N. D. Mathur, F. M. Grosche, S. R. Julian, I. R. Walker, D. M. Freye, R. K. W. Haselwimmer, and G. G. Lonzarich, Magnetically mediated superconductivity in heavy fermion compounds, Nature (London) **394**, 39 (1998).

[64] C. Petrovic, P. G. Pagliuso, M. F. Hundley, R. Movshovich, J. L. Sarrao, J. D. Thompson, Z. Fisk, and P. Monthoux, Heavy-fermion superconductivity in $CeCoIn_5$ at 2.3 K, J. Phys.: Condens. Matter **13**, L337 (2001).

[65] S. Nakatsuji, K. Kuga, Y. Machida, T. Tayama, T. Sakakibara, Y. Karaki, H. Ishimoto, S. Yonezawa, Y. Maeno, E. Pearson, G. G. Lonzarich, L. Balicas, H. Lee, and Z. Fisk, Superconductivity and quantum criticality in the heavy-fermion system β-$YbAlB_4$, Nat. Phys. **4**, 603 (2008).

[66] G. Knebel, D. Aoki, and J. Flouquet, Antiferromagnetism and superconductivity in cerium based heavy-fermion compounds, C. R. Phys. **12**, 542 (2011).

[67] S. Kasahara, T. Shibauchi, K. Hashimoto, K. Ikada, S. Tonegawa, R. Okazaki, H. Shishido, H. Ikeda, H. Takeya, K. Hirata, T. Terashima, and Y. Matsuda, Evolution from non-Fermi- to Fermi-liquid transport via isovalent doping in $BaFe_2(As_{1-x}P_x)_2$ superconductors, Phys. Rev. B **81**, 184519 (2010).

[68] A. E. Bohmer, P. Burger, F. Hardy, T. Wolf, P. Schweiss, R. Fromknecht, M. Reinecker, W. Schranz, and C. Meingast, Nematic Susceptibility of Hole-Doped and Electron-Doped $BaFe_2As_2$ Iron-Based Superconductors from Shear Modulus Measurements, Phys. Rev. Lett. **112**, 047001 (2014).

[69] T. Shibauchi, A. Carrington, and Y. Matsuda, A quantum critical point lying beneath the superconducting dome in iron pnictides, Annu. Rev. Condens. Matter Phys. **5**, 113 (2014).

[70] H.-H. Kuo, J.-H. Chu, J. C. Palmstrom, S. A. Kivelson, and I. R. Fisher, Ubiquitous signatures of nematic quantum criticality in optimally doped Fe-based superconductors, Science **352**, 958 (2016).

[71] J. Schmalian, D. Pines, and B. Stojkovic, Weak Pseudogap Behavior in the Underdoped Cuprate Superconductors, Phys. Rev. Lett. **80**, 3839 (1998).

[72] J. Schmalian, D. Pines, and B. Stojkovic, Microscopic theory of weak pseudogap behavior in the underdoped cuprate superconductors: General theory and quasiparticle properties, Phys. Rev. B **60**, 667 (1999).

[73] S. F. Edwards and P. W. Anderson, Theory of spin glasses, J. Phys. F: Met. Phys. **5**, 965 (1975).

[74] M. L. Mehta, *Random Matrices*, 3rd ed. (Elsevier, Amsterdam, 2004).

[75] We are grateful to an anonymous referee for pointing this out to us.

[76] P. B. Allen and R. C. Dynes, Transition temperature of strong-coupled superconductors reanalyzed, Phys. Rev. B **12**, 905 (1975).

[77] F. Marsiglio and J. P. Carbotte, Gap function and density of states in the strong-coupling limit for an electron-boson system, Phys. Rev. B **43**, 5355 (1991).

[78] A. E. Karakozov, E. G. Maksimov, and A. A. Mikhailovsky, The investigation of Eliashberg equations for superconductors with strong electron-phonon interaction, Solid State Commun. **79**, 329 (1991).

[79] R. Combescot, Strong-coupling limit of Eliashberg theory, Phys. Rev. B **51**, 11625 (1995).

[80] P. W. Anderson, Theory of dirty superconductors, J. Phys. Chem Solids **11**, 26 (1959).

[81] A. A. Abrikosov and L. P. Gor'kov, On the theory of superconducting alloys. 1. The electrodynamics of alloys at absolute zero, Zh. Eksp. Teor. Fiz. **35**, 1558 (1959) [Sov. Phys.–JETP **8**, 1090 (1959)].

[82] A. A. Abrikosov and L. P. Gor'kov, Superconducting alloys at finite temperatures, Zh. Eksp. Teor. Fiz. **36**, 319 (1959) [Sov. Phys.–JETP **9**, 220 (1959)].

[83] A. Abrikosov and L. P. Gor'kov, Contribution to the theory of superconducting alloys with paramagnetic impurities, Zh. Eksp. Teor. Fiz. **39**, 1781 (1961) [Sov. Phys.–JETP **12**, 1243 (1961)].

[84] A. C. Potter and P. A. Lee, Engineering a $p + ip$ superconductor: Comparison of topological insulator and Rashba spin-orbit-coupled materials, Phys. Rev. B **83**, 184520 (2011).

[85] J. Kang and R. M. Fernandes, Robustness of quantum critical pairing against disorder, Phys. Rev. B **93**, 224514 (2016).

[86] A. J. Millis, S. Sachdev, and C. M. Varma, Inelastic scattering and pair breaking in anisotropic and isotropic superconductors, Phys. Rev. B **37**, 4975 (1988).

[87] Ar. Abanov, A. V. Chubukov, and M. R. Norman, Gap anisotropy and universal pairing scale in a spin-fluctuation model of cuprate superconductors, Phys. Rev. B **78**, 220507(R) (2008).

[88] M. Langer, J. Schmalian, S. Grabowski, and K. H. Bennemann, Theory for the Excitation Spectrum of High-T_cSuperconductors: Quasiparticle Dispersion and Shadows of the Fermi Surface, Phys. Rev. Lett. **75**, 4508 (1995).

[89] J. Schmalian, M. Langer, S. Grabowski, and K. H. Bennemann, Self-consistent summation of many-particle diagrams on the real frequency axis and its application to the FLEX approximation, Comput. Phys. Commun. **93**, 141 (1996).

[90] Y.-M. Wu, A. Abanov, and A. V. Chubukov, Pairing in quantum critical systems: Transition temperature, pairing gap, and their ratio, Phys. Rev. B **99**, 014502 (2019).

[91] G. D. Mahan, *Many-Particle Physics*, 2nd ed. (Plenum, New York, 1993), Sec. 4.3.

[92] B. D. Josephson, Possible new effects in superconductive tunneling, Phys. Lett. **1**, 251 (1962).

[93] R. E. Harris, Cosine and other terms in the Josephson tunneling current, Phys. Rev. B **10**, 84 (1974).

[94] I. Esterlis, S. A. Kivelson, and D. J. Scalapino, A bound on the superconducting transition temperature, npj Quantum Mater. **3**, 59 (2018).

[95] Y. Wang, A Solvable Random Model with Quantum-critical Points for Non-Fermi-liquid Pairing, arXiv:1904.07240.